J. Fluid Mech. (2004), *vol.* 514, *pp.* 121–152.
DOI: 10.1017/S0022112004000187 Printed in the United Kingdom

Unsteady three-dimensional marginal separation caused by surface-mounted obstacles and/or local suction

By STEFAN BRAUN AND ALFRED KLUWICK

Institute of Fluid Mechanics and Heat Transfer, Vienna University of Technology, Resselgasse 3, A-1040 Vienna, Austria

(Received 25 July 2003 and in revised form 28 April 2004)

Earlier investigations of steady two-dimensional marginally separated laminar boundary layers have shown that the non-dimensional wall shear (or equivalently the negative non-dimensional perturbation displacement thickness) is governed by a nonlinear integro-differential equation. This equation contains a single controlling parameter Γ characterizing, for example, the angle of attack of a slender airfoil and has the important property that (real) solutions exist up to a critical value Γ_c of Γ only. Here we investigate three-dimensional unsteady perturbations of an incompressible steady two-dimensional marginally separated laminar boundary layer with special emphasis on the flow behaviour near Γ_c. Specifically, it is shown that the integro–differential equation which governs these disturbances if $\Gamma_c - \Gamma = O(1)$ reduces to a nonlinear partial differential equation – known as the Fisher equation – as Γ approaches the critical value Γ_c. This in turn leads to a significant simplification of the problem allowing, among other things, a systematic study of devices used in boundary-layer control and an analytical investigation of the conditions leading to the formation of finite-time singularities which have been observed in earlier numerical studies of unsteady two-dimensional and three-dimensional flows in the vicinity of a line of symmetry. Also, it is found that it is possible to construct exact solutions which describe waves of constant form travelling in the spanwise direction. These waves may contain singularities which can be interpreted as vortex sheets. The existence of these solutions strongly suggests that solutions of the Fisher equation which lead to finite-time blow-up may be extended beyond the blow-up time, thereby generating moving singularities which can be interpreted as vortical structures qualitatively similar to those emerging in direct numerical simulations of near critical (i.e. transitional) laminar separation bubbles. This is supported by asymptotic analysis.

1. Introduction

Marginal separation occurs in a variety of high-Reynolds-number flows. Probably the best known example is the incompressible flow past a slender airfoil at a small angle of attack where this phenomenon has been studied independently by Ruban (1981) and Stewartson, Smith & Kaups (1982) extending earlier work of Stewartson (1970) and Smith & Daniels (1981). Other examples include flows past backward facing steps, see e.g. Schlichting & Gersten (2000), flows past flared cylinders, Kluwick (1989), channel flows with suction, Hsiao & Pauley (1994), Alam & Sandham (2000) and viscous wall jets which are forced to change direction, Zametaev (1986). All these flows share the common property that solutions of the classical hierarchical

boundary-layer equations with imposed pressure distributions exist only up to a critical value of the controlling parameter, e.g. angle of attack, step height, flare angle, suction strength, deflection angle, etc. The limiting solution exhibits the remarkable feature that the wall shear vanishes in a single point, but immediately recovers. At the point of vanishing wall shear, the flow exhibits the marginal separation singularity characterized, among others, by the occurrence of a kink in the distribution of the wall shear stress and displacement thickness signalling a local breakdown of classical boundary-layer theory. For larger values of the controlling parameter, this breakdown manifests itself through the formation of a stronger singularity of the Goldstein type where the boundary-layer calculation comes to a definite end. However, as shown first by Ruban (1981) and Stewartson, Smith & Kaups (1982) by means of asymptotic analysis for large Reynolds numbers, the boundary-layer equations remain valid also for supercritical values of the controlling parameter and can be used to obtain uniformly valid approximations to the Navier–Stokes equations if the classical hierarchical concept of an imposed pressure distribution is given up and replaced by an interaction strategy. The essence of the analysis then is an integro–differential equation for the scaled wall shear as a function of the distance in the streamwise direction. It contains a single parameter Γ which measures the deviation from the critical value of the controlling parameter mentioned above. Both asymptotic analysis, Ruban (1981), and additionally numerical studies, Stewartson *et al.* (1982), presented in the original papers indicate that solutions to the interaction equation exist up to a critical value Γ_c of Γ only. Furthermore, Stewartson *et al.* (1982) who calculated Γ_c and Brown & Stewartson (1983) showed that two or even more different solutions exist in a certain range below Γ_c. The non-existence of steady solutions within the framework of predominately attached flows for values of Γ above Γ_c seems to indicate that a significant change of the flow field must take place as Γ passes through Γ_c. Further support for this conjecture was provided by Smith (1982) who investigated the response of two-dimensional marginally separated boundary layers to unsteady disturbances near or above Γ_c. It was found that the evolution of disturbances for $\Gamma > \Gamma_c$ inevitably lead to the formation of finite-time singularities. Their occurrence is preceded by a phase of rapid thickening of the boundary layer accompanied by substantial flow reversal which, as noted, qualitatively resembles early stages of dynamic stall before the shedding of a large eddy or vortex. Furthermore, analysis of terminal forms of the solutions indicated that the local breakdown is so severe that they are not influenced by the incident boundary layer in a leading-order approximation, suggesting in turn that such singular responses could arise in principle even for below-critical values of Γ. This was later confirmed by Ryzhov & Smith (1984) who then concluded that 'all marginal flows are very sensitive and should be considered to be in danger with regard to the unsteady stall process and the associated sudden change of the whole flow structure'. Similar conclusions were drawn by Duck (1990) dealing with unsteady three-dimensional marginal separation along a line of symmetry.

Little effort has been made so far to compare the predictions of the asymptotic theory of marginal separating flows and numerical solutions of the full Navier–Stokes equations. Probably the most comprehensive comparative study is that by Hsiao & Pauley (1994) who considered a two-dimensional laminar high-Reynolds-number channel flow. Suction was applied through a slot in the upper wall to generate a pressure distribution which forces the boundary layer forming on the lower wall to separate marginally. The Navier–Stokes calculations showed that the boundary layer became unstable near the reattachment point where separation occurred at high suction strength and oscillations of the wall shear near the reattachment point were

observed. As in Pauley, Moin & Reynolds (1990), this phenomenon was related to the onset of vortex shedding at which the boundary layer becomes unsteady and it was concluded that the critical value of Γ corresponds to the onset of vortex shedding. More recently, the DLR-TAU-code (a Reynolds-averaged Navier–Stokes code for steady three-dimensional flows using a pseudotime-stepping technique and Spalart–Almaras one-equation turbulence modelling, see e.g. Gerhold *et al.* 1997) was used by Braun, Kluwick & Trenker (2003) to calculate solutions of the Navier–Stokes equations for two-dimensional steady flows past slender airfoils. Specifically, the airfoil thickness was taken to be 10% of the chord length $\bar{L}$ and the Reynolds number of 20 000 based on $\bar{L}$ was considered as a compromise between the rapidly growing computational effort and the validity of the asymptotic theory. Converged solutions could be obtained up to a maximum angle of attack $\alpha_m = 4.25^\circ$ which agrees very well with the value $\alpha_m = 4.44^\circ$ predicted by the theory of marginal separation. In this connection, note that classical boundary-layer theory has already broken down for $\alpha_c = 3.37^\circ$ which indicates that the applicability of the boundary-layer concept can be extended significantly by adopting an interaction strategy. Also, it should be noted that laminar–turbulent transition within the boundary layer had to be allowed for in the numerical calculations to obtain steady solutions. Convergence for $\alpha \approx \alpha_m$ could be achieved only if transition was assumed to occur approximately at the location of the laminar separation bubble. This observation appears to be in line with earlier experimental and numerical work (albeit for simpler geometries) indicating the possibility that laminar separation bubbles may trigger the transition process (e.g. Alam & Sandham 2000; Theofilis 2003). It finds further support from the study of Mary & Sagaut (2002) which to the authors' knowledge represents the first satisfying large eddy simulation of the complex flow past an airfoil. In view of the work just mentioned, the asymptotic theory of marginal separation appears to be confronted with the following questions:

(i) Does the passage through Γ_c indeed lead to a completely different flow structure or is it associated with much milder changes of the flow behaviour (as suggested by the results reported by Hsiao & Pauley 1994)?

(ii) Can a description of (the early stages of) the transition process triggered by laminar separation bubbles be extracted from the theory and what role do finite-time singularities predicted among others by Smith (1982), Ryzhov & Smith (1984), Smith & Elliott (1985), Elliott & Smith (1987), and Duck (1990) play in this connection?

(iii) Can the occurrence of these phenomena be delayed by increasing the value of Γ_c through the application of so-called smart devices, for example, by surface-mounted obstacles and suction stripes?

In general, the investigation of these questions will require the numerical solution of the full nonlinear interaction equation suitably generalized to account for the effect of unsteady three-dimensional disturbances and smart devices which represents a formidable task. However, as shown by Braun & Kluwick (2002*a*, 2003) for steady flows, the treatment of the interaction equation can be simplified considerably if Γ deviates only slightly from the critical value Γ_c. This and the preliminary study by Braun & Kluwick (2002*b*) suggests that a similar approach might be useful to make the problem under consideration more tractable, which is the aim of the present investigation.

Following the problem formulation in § 2, a simplified form of the interaction equation holding in the limit $\Gamma_c - \Gamma \to 0$ is derived in § 3 which describes the evolution of three-dimensional unsteady disturbances superimposed on a two-dimensional steady marginally separated boundary layer. Using both analytical and numerical

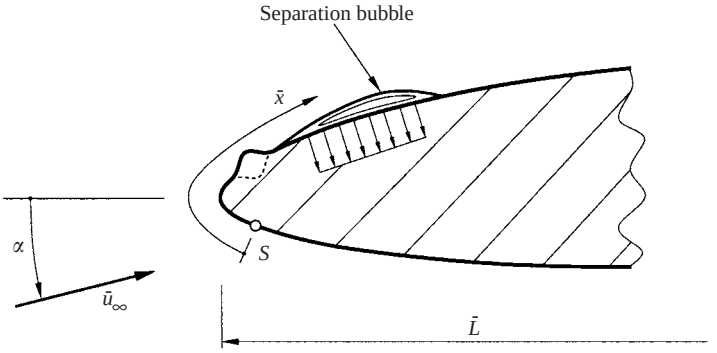

FIGURE 1. Flow control by means of 'smart structures': manipulation of leading-edge separation using surface-mounted obstacles and/or suction. Boundary-layer coordinate $\bar{x}$ measured from stagnation point S.

methods, solutions to this equation are obtained in § 4 and discussed in physical terms. Section 5 is devoted to aspects of flow control with special emphasis on the effects caused by surface-mounted obstacles and suction/blowing stripes. Finally, concluding remarks and possible trends of future work are summarized in § 6.

2. Problem formulation

Consider the planar incompressible steady and laminar high-Reynolds-number flow around the leading edge of a thin airfoil at a small angle of attack α (figure 1). As pointed out before, we concentrate on the limiting case $\alpha \simeq \alpha_c$, where the classical boundary-layer calculation yields a marginal separation singularity at $x = x_0$ on the suction side and the interaction between the local thickening of the boundary layer and the feedback effect of the induced pressure in the outer inviscid flow field can no longer be neglected. Special emphasis is placed on the investigation of the effect of three-dimensional unsteady disturbances imposed in the form of surface-mounted obstacles and/or suction/blowing distributions on the interaction process. Field variables and coordinates non-dimensionalized with appropriate reference quantities (subscript ∞) such as the chord length $\bar{L}$ and the free-stream velocity $\bar{u}_\infty$ are defined as

$$\left.\begin{aligned} &(x, y, z) = \frac{1}{\bar{L}}(\bar{x}, \bar{y}, \bar{z}), \quad t = \frac{\bar{u}_\infty \bar{t}}{\bar{L}}, \quad \boldsymbol{u} = (u, v, w) = \frac{1}{\bar{u}_\infty}(\bar{u}, \bar{v}, \bar{w}), \\ &p = \frac{\bar{p} - \bar{p}_\infty}{\bar{\rho}_\infty \bar{u}_\infty^2}, \quad (\tau_x, \tau_z) = \frac{\bar{L}}{\bar{\rho}_\infty \bar{\nu}_\infty \bar{u}_\infty}(\bar{\tau}_x, \bar{\tau}_z), \end{aligned}\right\} \tag{2.1}$$

where x, y and z denote Cartesian coordinates in the streamwise direction, normal to the wall and in the spanwise direction, u, v, w and τ_x, τ_z the corresponding velocity and shear stress components. Further, t, p, ρ and ν represent the time, pressure, density and kinematic viscosity. The governing Navier–Stokes equations may then be written in the form

$$\frac{\partial \boldsymbol{u}}{\partial t} + (\boldsymbol{u} \cdot \nabla)\boldsymbol{u} = -\nabla p + \frac{1}{Re}\Delta \boldsymbol{u}, \quad \nabla \cdot \boldsymbol{u} = 0, \quad Re = \frac{\bar{u}_\infty \bar{L}}{\bar{\nu}_\infty} \to \infty, \tag{2.2}$$

subjected to the no-slip boundary condition $\boldsymbol{u} = (0, v_w, 0)$ imposed at the solid wall $y = 0$. Here, Re is the Reynolds number and $v_w(x, z, t)$ denotes the distribution of the suction velocity prescribed at the surface.

Proper expansions in the lower deck (subscript 2) of the three-tiered interaction regime are

$$\left.\begin{aligned} u_2 &\sim Re^{-1/10}\frac{p_{00}}{2}y_2^2 + Re^{-1/4}A_1(s_2, z_2, t_2)y_2 + \cdots + Re^{-2/5}u_{22}(s_2, y_2, z_2, t_2) + \cdots,\\ v_2 &\sim Re^{-6/10}\frac{\partial}{\partial s_2}(-A_1 + p_{00}h(s_2, z_2, t_2))\frac{y_2^2}{2} + \cdots + Re^{-3/4}v_{22}(s_2, y_2, z_2, t_2) + \cdots,\\ w_2 &\sim Re^{-2/5}w_{20}(s_2, y_2, z_2, t_2) + \cdots,\\ \nabla p_2 &\sim p_{00}\boldsymbol{e}_x + \cdots + Re^{-3/10}\nabla_2 p_2^i(s_2, z_2, t_2) + \cdots, \end{aligned}\right\} \tag{2.3}$$

where

$$\left.\begin{aligned} x &= x_0 + Re^{-1/5}s_2, \quad y = Re^{-11/20}y_2 + Re^{-7/10}h,\\ z &= Re^{-1/5}z_2, \quad t = Re^{1/20}t_2, \end{aligned}\right\} \tag{2.4}$$

are the corresponding stretched coordinates (notation and scalings are taken from Braun & Kluwick 2002*a*). To affect the wall shear or equivalently the correction to the negative displacement thickness A_1, which is determined by the solvability condition of the second-order problem, the height $\bar{h}$ of a surface-mounted obstacle and the intensity of the suction/blowing velocity $\bar{v}_w$ have to be of the orders $Re^{-7/10}\bar{L}$ (Hackmüller & Kluwick 1991), and $Re^{-3/4}\bar{u}_\infty$ (Hackmüller & Kluwick 1990), respectively:

$$\frac{\bar{h}}{\bar{L}} = Re^{-7/10}h, \quad \frac{\bar{v}_w}{\bar{u}_\infty} = Re^{-3/4}v_w. \tag{2.5}$$

The latter requirement can be inferred directly by inspecting the second line of (2.3). Similar arguments hold for the inclusion of unsteady effects leading to the slow time scale given in (2.4), Smith (1982) and Ruban (1983).

Application of the solution procedure introduced by Stewartson (1970), taking into account the coupling condition between A_1 and the induced pressure p_2^i as given from the solution of the upper-deck problem, the boundary and various matching conditions within the triple-deck regime, yields, after the usual affine transformations given, for example, in Braun & Kluwick (2002*a*) and supplemented with

$$t_2 = a_0^{-9/10}p_{00}^{3/10}U_{00}^{-1/5}T, \quad v_w \to a_0^{3/2}p_{00}^{-3/2}U_{00}v_w, \tag{2.6}$$

the solvability condition or fundamental equation for the wall shear $A(X, Z, T)$

$$\begin{aligned} A^2 - X^2 + \Gamma = \frac{\lambda}{2\pi}\int_{-\infty}^{X}\frac{\mathrm{d}s}{\sqrt{X-s}}\int_{-\infty}^{\infty}\int_{-\infty}^{\infty}\frac{1}{\sqrt{(s-\xi)^2 + (Z-\eta)^2}}\\ \times\left(\frac{\partial^3}{\partial\xi^3} + \frac{\partial^3}{\partial\xi\,\partial\eta^2}\right)(A-h)\,\mathrm{d}\xi\,\mathrm{d}\eta\\ -\gamma\int_{-\infty}^{X}\frac{1}{(X-\xi)^{1/4}}\frac{\partial(A-h)}{\partial T}\,\mathrm{d}\xi - \kappa\int_{-\infty}^{X}\frac{v_w}{(X-\xi)^{1/4}}\,\mathrm{d}\xi, \end{aligned} \tag{2.7}$$

with the positive constants

$$\lambda = \frac{\left(-\frac{1}{4}\right)!}{\sqrt{2}\left(\frac{1}{4}\right)!}, \quad \gamma = \frac{2^{3/4}}{\left(-\frac{3}{4}\right)!}, \quad \kappa = \frac{2^{3/4}}{\left(\frac{1}{4}\right)!}. \tag{2.8}$$

The constants $U_{00}=u_e(x_0)$, $p_{00}=-u_e u_e'|_{x=x_0}>0$ and $a_0=\lim_{x\to x_0^{\pm}}|\tau_{wx}'|$ represent the velocity of the outer inviscid flow field, the pressure gradient and the slope of the wall shear stress as given from the classical boundary-layer calculation at the separation point $x=x_0$. Further, $\Gamma\propto Re^{2/5}(\alpha-\alpha_c)\sim O(1)$ denotes the scaled deviation from the critical angle of attack.

The counterpart of (2.7) for strictly planar flow, i.e. $\partial/\partial Z=0$, is given by

$$A_\infty^2-X^2+\Gamma=\lambda\int_X^\infty\frac{1}{\sqrt{\xi-X}}\frac{\partial^2(A_\infty-h_\infty)}{\partial\xi^2}\,\mathrm{d}\xi$$
$$-\gamma\int_{-\infty}^X\frac{1}{(X-\xi)^{1/4}}\frac{\partial(A_\infty-h_\infty)}{\partial T}\,\mathrm{d}\xi-\kappa\int_{-\infty}^X\frac{v_{w\infty}}{(X-\xi)^{1/4}}\,\mathrm{d}\xi\,; \qquad (2.9)$$

here, and in the following, the corresponding quantities are indicated by the subscript ∞. Since h and v_w represent local effects, they do not affect the far-field behaviour of the wall shear A (proportional to A_1) with respect to the streamwise coordinate X to leading order which is given by $A(X,Z,T)\sim A_\infty(X,T)\sim|X|$ as $X\to\pm\infty$.

Equations (2.7) and (2.9) have to be solved numerically, in general, which requires considerable computational effort (cf. Smith 1982; Duck 1990). As outlined in these two papers, it is also possible to allow for the (slow) time dependence of the angle of attack parameter Γ to be taken into account, for example, the pitching motion of an airfoil. In the present investigation however, we, restrict ourselves to the case $\Gamma=const.$

Important and well-known features of (2.7) and (2.9) are the existence of an upper bound Γ_c of Γ, up to which steady solutions can be found and the non-uniqueness of the solutions for $0<\Gamma<\Gamma_c$. In the following, we focus on the properties of solutions to these equations in the limit of small deviations of Γ from its critical value Γ_c where analytical progress is possible.

3. Bifurcation near the critical angle of attack

The subsequent derivation of asymptotic solutions of (2.7) in the limit $\Gamma\to\Gamma_c$ is largely based on earlier papers (Braun & Kluwick 2002*a*, 2003) where several steps are outlined in more detail.

3.1. *Asymptotic expansion of the fundamental equation*

Introducing the definition $\Gamma_c-\Gamma=\varepsilon^4\to0^+$ and the appropriate scalings $A(X,\varepsilon Z,\varepsilon^2T)=\bar A(X,\bar Z,\bar T)$ for the spanwise coordinate and the time, the almost parabolic shape of the relationship between $A_\infty(0)$ and Γ near the bifurcation point $\Gamma=\Gamma_c$ and numerical findings concerning the behaviour of steady three-dimensional disturbances associated with upper- and lower-branch solutions suggest the expansion

$$\bar A\sim A_{\infty c}(X)+\varepsilon^2a_1(X,\bar Z,\bar T)+\cdots. \qquad (3.1)$$

The leading-order term $A_{\infty c}$ is given by the steady solution for strictly planar flow at the branching point Γ_c and the unsteady three-dimensional correction a_1 is represented by a Fourier-integral with respect to the spanwise coordinate

$$a_1=\int_0^\infty[\hat a(X,k,\bar T)\cos(k\bar Z)+\hat b(X,k,\bar T)\sin(k\bar Z)]\,\mathrm{d}k. \qquad (3.2)$$

Insertion of (3.1) and (3.2) into (2.7), taking into account that perturbations of the steady two-dimensional forms of the obstacle shape and the suction distribution

compatible with the present asymptotic analysis are of $O(\varepsilon^4)$:

$$h = h_\infty(X) + \varepsilon^4 h_1(X, \bar{Z}, \bar{T}), \quad v_w = v_{w\infty}(X) + \varepsilon^4 v_{w1}(X, \bar{Z}, \bar{T}), \tag{3.3}$$

shows that $a_1(X, \bar{Z}, \bar{T})$ can be written as the product of two functions $b(X)\,c(\bar{Z}, \bar{T})$ and indicates the structure of higher-order terms in the expansion for the wall shear

$$\bar{A} \sim A_{\infty c}(X) + \varepsilon^2 b(X) c(\bar{Z}, \bar{T}) + \varepsilon^4 [\ln \varepsilon\, b(X) d(\bar{T}) + a_2(X, \bar{Z}, \bar{T})] + O(\varepsilon^6 \ln^2 \varepsilon). \tag{3.4}$$

It is convenient to introduce the following abbreviations for the integral operators

$$I\cdot = \lambda \int_X^\infty \frac{1}{\sqrt{\xi - X}} \frac{\partial^2 \cdot}{\partial \xi^2}\, \mathrm{d}\xi, \quad J\cdot = \lambda \int_X^\infty \frac{\cdot\, \mathrm{d}\xi}{\sqrt{\xi - X}}, \quad K\cdot = \gamma \int_{-\infty}^X \frac{\cdot\, \mathrm{d}\xi}{(X - \xi)^{1/4}}. \tag{3.5}$$

The staggered system of equations for the coefficient functions $A_{\infty c}$, b, c and d then takes on the form given below. Planar obstacles and suction distributions determine the value of Γ_c through the leading-order problem

$$A_{\infty c}^2 - X^2 + \Gamma_c = I(A_{\infty c} - h_\infty) - \frac{\kappa}{\gamma} K v_{w\infty}. \tag{3.6}$$

In § 5, we demonstrate the possibility of exceeding the value $\Gamma_c \approx 2.66$ arising in the case of a locally plane and impermeable wall through suitable choices of h_∞ and $v_{w\infty}$. Corrections of the wall shear for planar flow caused by small deviations of Γ from Γ_c are accounted for by the right eigenfunction $b(X)$

$$(2A_{\infty c} - I)b = 0, \tag{3.7}$$

see figure 16. Its asymptotic behaviour, calculated in Braun & Kluwick (2003)

$$\left.\begin{aligned} &b(X \to -\infty) \sim b^-\,(-X)^{-7/2}, \\ &b(X \to \infty) \sim b^+ \int_0^\infty \exp\left(-ar^{5/2}\right) \cos\left(ar^{5/2} + rX\right) \mathrm{d}r, \quad a = \frac{\lambda}{5}\sqrt{\frac{\pi}{2}}, \end{aligned}\right\} \tag{3.8}$$

with $b^- \approx 1.54$ and $b^+ \approx 45.0$ is essential for the derivation of expansion (3.4). As a consequence of (3.7), the X-dependence of the wall shear disturbances is uniquely determined by the properties of the unperturbed flow and thus cannot be adjusted to arbitrary initial conditions. This obviously reflects the fact, known from other studies of marginally separated flows (e.g. Ryzhov & Smith 1984; Smith & Elliott 1985), that the Cauchy problem associated with the unsteady version of the interaction equation is ill-posed, in general, owing to the unbounded growth of perturbations from the large wavenumber spectrum. One possibility for regularizing the problem, which has been suggested before, is to solve the Cauchy problem with 'filtered' initial data, but how to choose the appropriate filter remained unclear. In contrast, the present approach yields the proper regularization as part of the solution. Since $|b(X)|$ is integrable from $-\infty$ to ∞, it follows from the lemma of Riemann–Lebesgue (see e.g. Lighthill 1958) that the Fourier transform $\tilde{b}(k) \to 0$ as $|k| \to \infty$ thereby avoiding the large-wavenumber catastrophe. It should be noted, however, that this does not prevent the study of flows resulting from the presence of arbitrary obstacle shapes and suction velocities. Within the framework of the present theory, forcings of different form lead, in general, to a different evolution of the wall shear in $\bar{Z}$ and $\bar{T}$ while its X-dependence is universal.

Following the lines of the analysis presented in Braun & Kluwick (2003), it is easily shown that unsteady three-dimensional contributions are governed by the nonlinear evolution equation for the shape function c

$$\frac{\partial c}{\partial \bar{T}} - \nu \frac{\partial^2 c}{\partial \bar{Z}^2} + \mu c^2 - \delta = \bar{g}(\bar{Z}, \bar{T}), \tag{3.9}$$

with the constant coefficients ν, μ, δ and the forcing term $\bar{g}$ given by

$$\nu = \frac{\langle n, Jb\rangle}{2\langle n, Kb\rangle}, \quad \mu = \frac{\langle n, b^2\rangle}{\langle n, Kb\rangle}, \quad \delta = \frac{\langle n, 1\rangle}{\langle n, Kb\rangle}, \quad \bar{g} = -\frac{\gamma\langle n, Ih_1\rangle + \kappa\langle n, Kv_{w1}\rangle}{\gamma\langle n, Kb\rangle}. \tag{3.10}$$

Here, and in the following, the notation

$$\langle n, q\rangle := \int_{-\infty}^{\infty} nq \, \mathrm{d}X \tag{3.11}$$

is used for the scalar product of functions and $n(X)$ represents the non-unique left eigenfunction of the integral operator given in (3.7) (Braun & Kluwick 2002*a*, 2003). Without loss of generality, we impose the normalization condition $\langle n, 1\rangle = 1$. Numerical calculations yield the values $\nu \approx 3.0$, $\mu \approx 2.07$ and $\delta \approx 1.60$ in the case of $h_\infty = v_{w\infty} = 0$. The stationary points of the nonlinear evolution equation (3.9) corresponding to planar upper- and lower-branch solutions are denoted by $\pm c_s$ where $c_s = \sqrt{\delta/\mu}$.

The calculation of the next higher contribution $d(\bar{T})$ to the wall shear is given in the Appendix. In passing, we also note that the perturbation scheme applied in § 3.1 exhibits certain similarities with the reductive perturbation approach of Taniuti & Wei (1968) for the treatment of weakly nonlinear hyperbolic waves. There, the first-order solution vector can be written as the product of the right eigenvector associated with a homogeneous set of linear equations and a function of time satisfying a solvability condition which results from the inspection of higher-order terms.

3.2. *Flow field quantities*

The analysis carried out so far indicates that the intensive numerical computation efforts required to obtain solutions of (2.7) or (2.9) can be reduced substantially if Γ deviates only slightly from the critical value Γ_c. Also, by expanding the wall shear stress in the form (3.4), the main flow characteristics become visible more clearly since they express themselves in the form of the significantly simpler equations (3.6), (3.7), (3.9) and (A 2). In this connection, it is interesting to determine also the associated asymptotic structure of other field quantities such as the induced pressure disturbances and the lateral component of the wall shear which provide not only further insight into the flow behaviour, but may be useful also for future comparison with experimental data or results of numerical calculations based on the full equation (2.7).

The coupling condition between the displacing effect of the viscous sublayer and the feedback pressure $P \propto p_2^i$ following from the upper-deck solution is given by

$$P(X, Z, T) = -\frac{1}{2\pi} \int_{-\infty}^{\infty} \int_{-\infty}^{\infty} \frac{1}{\sqrt{(X-\xi)^2 + (Z-\eta)^2}} \frac{\partial^2 (A-h)}{\partial \xi^2} \, \mathrm{d}\xi \, \mathrm{d}\eta, \tag{3.12}$$

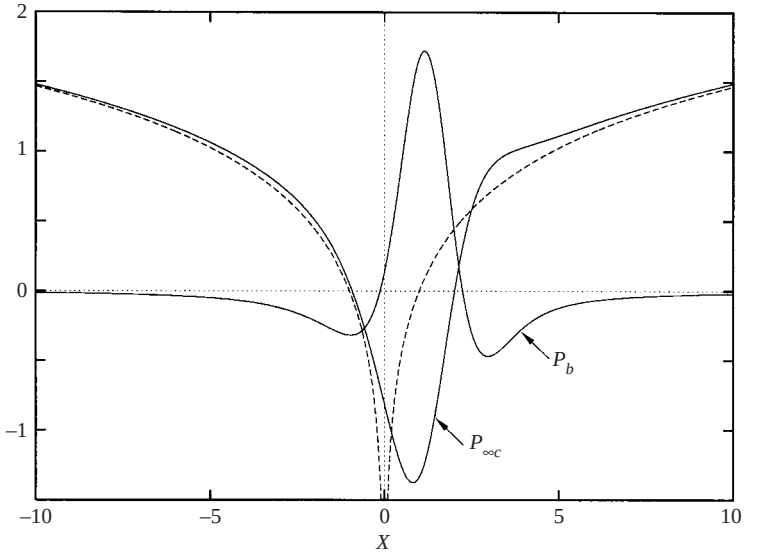

FIGURE 2. Interaction pressure distribution near the critical angle of attack, equation (3.13) with $h_\infty = v_{w\infty} = 0$. Dashed lines: far-field asymptotes (3.14).

which on substituting (3.4) leads to the expression

$$\left.\begin{aligned} &\bar{P}(X,\bar{Z},\bar{T}) \sim P_{\infty c} + (\varepsilon^2 c + \varepsilon^4 \ln\varepsilon\, d)P_b + O(\varepsilon^4),\\ &P_{\infty c}(X) = \frac{1}{\pi}\int_{-\infty}^{\infty} \frac{(A_{\infty c} - h_\infty)'}{X-\xi}\,\mathrm{d}\xi, \quad P_b(X) = \frac{1}{\pi}\int_{-\infty}^{\infty} \frac{b'}{X-\xi}\,\mathrm{d}\xi. \end{aligned}\right\} \tag{3.13}$$

The far-field behaviour of $P_{\infty c}$ is given by Hadamard's finite part of the corresponding divergent integral in (3.13) and that of P_b can be obtained by the method applied in the Appendix of the paper by Braun & Kluwick (2003),

$$P_{\infty c} \sim \frac{2}{\pi}\ln|X| + \cdots, \quad P_b \sim O(X^{-2}), \quad X \to \pm\infty, \tag{3.14}$$

see figure 2.

It is difficult to measure wall shear stresses directly, in particular near separation where their magnitude is small. Instead, oil coatings are often used to visualize the wall streamlines near separated flow regions. These can easily be calculated within the framework of the present study. To this end, the leading-order contributions of the wall shear components

$$\left.\begin{aligned} &\tau_{wx} = \left(Re^{11/20}\frac{\partial u_2}{\partial y_2} + Re^{1/5}\frac{\partial v_2}{\partial s_2}\right)\Bigg|_{y_2=0} \sim Re^{3/10}a_0^{3/5}p_{00}^{-1/5}U_{00}^{4/5}A_{\infty c} + O(\varepsilon^2),\\ &\tau_{wz} = \left(Re^{11/20}\frac{\partial w_2}{\partial y_2} + Re^{1/5}\frac{\partial v_2}{\partial z_2}\right)\Bigg|_{y_2=0} \sim Re^{3/20}a_0^{13/10}p_{00}^{-11/20}U_{00}^{7/5}\varepsilon^3\frac{\partial c}{\partial \bar{Z}}\Upsilon + O(\varepsilon^5),\\ &\Upsilon(X) = -\frac{\left(\frac{1}{2}\right)!\left(-\frac{1}{4}\right)!}{2^{1/4}\pi}\int_{-\infty}^{X}\frac{P_b}{(X-\xi)^{3/4}}\,\mathrm{d}\xi \end{aligned}\right\} \tag{3.15}$$

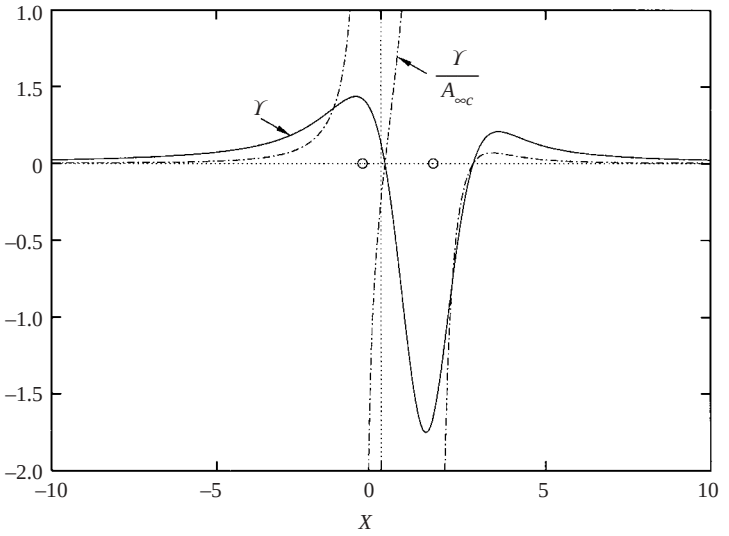

FIGURE 3. Leading-order X-dependence of the wall shear stress τ_{wz} and slope $\mathrm{d}\bar{Z}/\mathrm{d}X$ of wall streamlines, (3.16). Open circles denote leading-order separation and reattachment lines ($h_\infty = v_{w\infty} = 0$).

are inserted into the differential equation $\mathrm{d}x/\mathrm{d}z = \tau_{wx}/\tau_{wz}$ to give

$$\frac{\mathrm{d}\bar{Z}}{\mathrm{d}X} \sim Re^{-3/20} a_0^{7/10} p_{00}^{-9/10} U_{00}^{3/5} \varepsilon^4 \frac{\Upsilon}{A_{\infty c}} \frac{\partial c}{\partial \bar{Z}} + O(\varepsilon^6), \tag{3.16}$$

see figure 3.

Surface plots of constant vorticity are usually used to illustrate computational fluid dynamics results, especially if vortical structures appear, as for example, in the near wall regime of transitional separation bubbles. In the lower deck, the vorticity vector $\boldsymbol{\omega} = \nabla \times \boldsymbol{u}$ is given by

$$\boldsymbol{\omega} = \begin{pmatrix} Re^{3/20} \dfrac{\partial w_{20}}{\partial y_2} + O\left(Re^{-2/5}\right) \\ Re^{-1/20} \dfrac{\partial A_1}{\partial z_2} y_2 + O\left(Re^{-1/5}\right) \\ -Re^{9/20} p_{00} y_2 - Re^{3/10} A_1 + O\left(Re^{3/20}\right) \end{pmatrix}, \tag{3.17}$$

which shows that A_1 represents the leading-order correction of the vorticity component in spanwise direction.

4. The bursting process and the generation of vortex sheets

In this section, our main interest is the nonlinear evolution equation (3.9). To eliminate various constants the transformation

$$c(\bar{Z}, \bar{T}) + c_s = 2c_s u(z, t), \quad \bar{Z} = \sqrt{\frac{\nu}{2\mu c_s}}\, z, \quad \bar{T} = \frac{t}{2\mu c_s} \tag{4.1}$$

is applied to end up with the forced Fisher equation (Fisher 1937)

$$\frac{\partial u}{\partial t} - \frac{\partial^2 u}{\partial z^2} = u - u^2 + g(z, t), \tag{4.2}$$

with the forcing term $g = \bar{g}/(4\delta)$. The stationary points $u_s = (0, 1)$ of the unforced equation (4.2) describe the lower- and upper-branch solutions associated with steady planar flow. Their stability properties can be determined from a linear analysis based on the ansatz $u(z, t) = u_s + \Delta u \exp(\mathrm{i}kz + \omega t)$ where $|\Delta u| \ll 1$, k and ω denote the (small) amplitude, the wavenumber and the angular frequency, respectively. We then obtain the dispersion relations $\omega = 1 - k^2$ for $u_s = 0$ and $\omega = -1 - k^2 < 0$ for $u_s = 1$ indicating that lower-/upper-branch solutions are unstable/stable in general. Equations of Fisher's type (heat equations with nonlinear source terms) are known from the description of nonlinear wave propagation phenomena in gene populations, reaction-diffusion and heat conduction processes. Its appearance in the context of marginal separation forms one of the key results of the present investigation. In contrast to studies dealing with the temporal evolution of gene populations, reactant concentrations or temperature distributions where the concentration or temperature $u(z, t)$ is limited to positive values within the range $[0, 1]$ or $[0, \infty)$ no restrictions on the magnitude and sign of u exist in the present case. As a consequence, given smooth and bounded initial data may not only evolve into bounded solutions, but may also lead to a blow-up of the solutions within finite time, indicating the bursting of the separation bubble associated with the ejection of near wall fluid out of the boundary layer. For a general introduction into the subject of singularity formation in the solution of nonlinear parabolic equations the reader is referred to the surveys given in Galaktionov & Vazquez (2002) and Samarskii *et al.* (1995).

To obtain some first insight, it is useful to consider the simplest case of unforced planar flow with the initial condition $u(t_0) = u_0 = const$, where (4.2) can be solved analytically,

$$u(t) = \frac{u_0 + u_0 \tanh[(t - t_0)/2]}{1 + (2u_0 - 1)\tanh[(t - t_0)/2]}. \tag{4.3}$$

For $u_0 > 0$, the steady planar upper-branch solution $u_s = 1$ is approached as $t \to \infty$, whereas for values of u_0 below the lower branch $u_s = 0$, finite-time blow-up occurs at the blow-up time

$$t^* = t_0 + 2\,\mathrm{artanh}[1/(1 - 2u_0)], \tag{4.4}$$

(see figure 4). Surprisingly, however, this blow-up does not terminate the solution which, in fact, can be continued beyond t^* where it approaches the stable upper branch asymptotically in the limit $t \to \infty$. The possibility of continuing solutions of the interaction equation (2.7) or its two-dimensional counterpart (2.9) beyond finite-time blow-up apparently has not been recognized so far. The exploration of this phenomenon also under conditions which are more general than those leading to (4.3) is one of the main aims of the present study. To this end, we continue with the description of some numerical experiments which, in fact, provided the first hints of the possibility of extending solutions beyond the blow-up time.

4.1. *Numerical experiments*

An implicit Euler finite-differencing scheme (first-order backward and second-order accurate centred difference formulae for the time and spatial derivatives, respectively, and Taylor series expansion of the nonlinear term at the previous time step) is applied

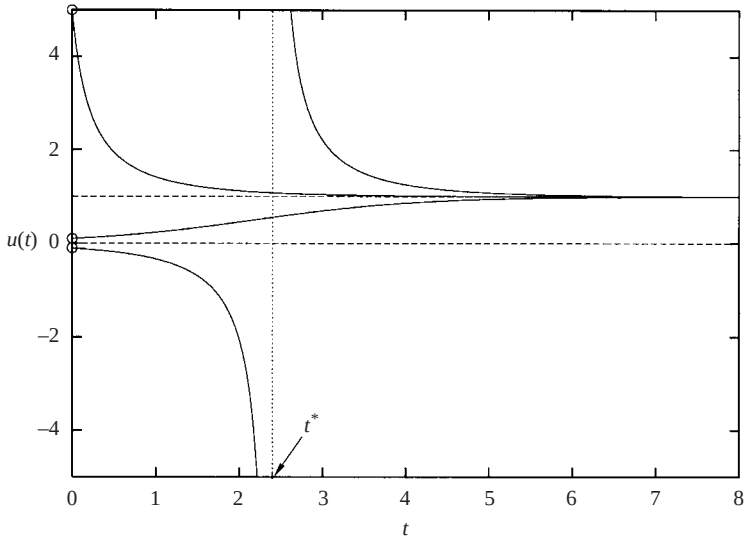

FIGURE 4. Solutions of Fisher's equation (4.2) for planar flow without forcing. Open circles denote the different initial conditions $u(t_0=0)=u_0=(-0.1, 0.1, 5)$, dashed lines: stationary states $u_s=(0, 1)$, blow-up time t^*.

to (4.2), leading to the tri-diagonal linear equation system

$$-\frac{u_{i-1,j}}{\Delta z^2}+\left(\frac{1}{\Delta t}+\frac{2}{\Delta z^2}+2u_{i,j-1}-1\right)u_{i,j}-\frac{u_{i+1,j}}{\Delta z^2}=\frac{u_{i,j-1}}{\Delta t}+u_{i,j-1}^2+g_{i,j}, \tag{4.5}$$

which is solved using the Thomas algorithm. Here, $\Delta z=2L/N$ and Δt denote the step sizes of the computational domain $z\in[-L, L]$ and $u(z, t)\to u_{i,j}=u(i\Delta z-L, j\Delta t)$ with $i=0, 1, \cdots, N$ and $j=0, 1, \cdots$. In the following examples, the initial condition is chosen to be the stable planar upper-branch solution, i.e. $u(z, 0)=1$ and typical step sizes are of the order $\Delta t\sim O(\Delta z^2)\approx(10^{-4}\ldots 10^{-6})$. The forcing term is assumed to be of the form

$$g(t)=a\ \sin(\omega t)\,\theta(t), \tag{4.6}$$

$$g(z, t)=a\ \sin(\omega t)\,\mathrm{e}^{-(z/B)^2}\,\theta(t), \tag{4.7}$$

for planar and three-dimensional flow, respectively, and therefore corresponds to vibrating surface-mounted obstacles or periodic alternating suction/blowing distributions. Here, a is the forcing amplitude, ω the angular frequency, B a typical extent of the three-dimensional disturbance in spanwise direction and $\theta(t)$ denotes Heaviside's step function. Note that the assumed form of the forcing (4.7) leads to the symmetry property $u(z, t)=u(-z, t)$.

Figure 5 displays numerical solutions for planar flow. Depending on the magnitude of the parameter a relative to a critical value $a_c(\omega)$, completely different situations arise. For $a<a_c$, a constant response amplitude and phase shift of u with respect to g is obtained after some time. In this context, note the possible extension of the values of u into the unstable regime $u<0$, i.e. the delay of the stall phenomena through transient mechanisms ('dynamic stall'). On the other hand, a slight increase of a beyond a_c leads to a growth of the response amplitude until nonlinear effects dominate the evolution process and eventually cause the bursting of the separation bubble at a finite time t^*. However, a continuation of the solution beyond the blow-up time t^* is found

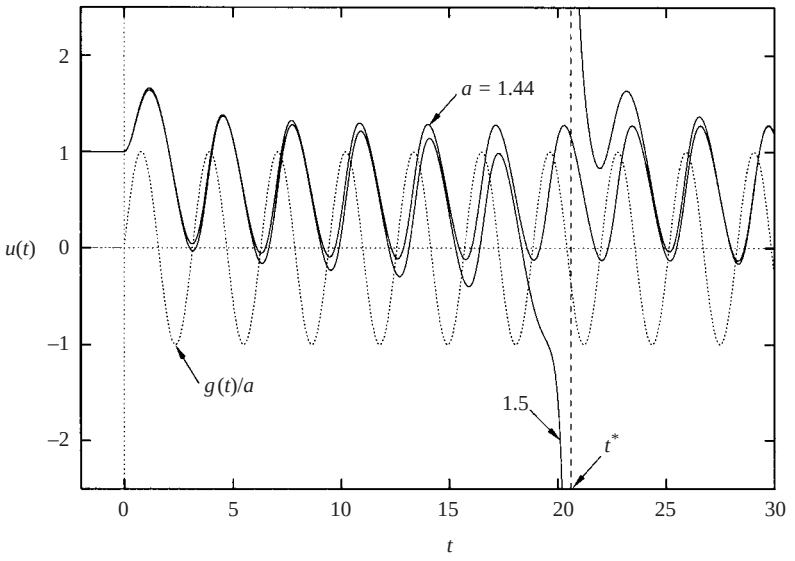

FIGURE 5. Temporal evolution of the scaled wall shear contribution $u(t)$ for planar flow due to forcing (4.6) with $\omega = 2$. For amplitudes larger than $a_c \approx 1.44$ repeated bubble bursting occurs (blow-up time t^*).

to be possible provided that the step size Δt in the numerical scheme is kept fixed and is not refined until the restricted machine precision terminates the calculation before t^*. Similar to the analytical result (4.3) for unforced flows this continuation is accompanied with the occurrence of a pole-like singularity which triggers the initial phase of boundary-layer recovery for $t > t^*$. The presence of the forcing term (4.6), however, prevents a full recovery of the boundary layer, but causes the formation of another finite-time singularity leading eventually to an almost periodic process of repeated bubble bursting. As an essential result we therefore conclude that the bursting process is a temporary phenomenon which is associated with the release of a planar vortex sheet.

Finite-time blow-up is obtained also in the case of three-dimensional flow as can be seen if the numerical solution resulting from the forcing (4.7) is plotted along the axis $z = 0$. Here, we turn our attention to the blow-up profiles, i.e. curves $u(z, t)$ for fixed t near t^*. For $t < t^*$, a pronounced focusing of the solution in the form of a rapid increase of the amplitude at $z = 0$ is obtained (figure 6). Beyond t^*, a characteristic pattern appears which moves away from the $z = 0$ axis. Its qualitative shape and movement is seen to be reliable with respect to changes in the step sizes. The large amplitudes of this moving pattern point to the generation of a pair of moving singularities immediately beyond blow-up which is supported by asymptotic analysis and interpreted as the creation of Λ-vortices. A comparison between the numerical results and the asymptotic prediction is given in figures 7 to 9.

Although the numerical scheme seems to accomplish the transition through the blow-up point, it cannot, of course, handle moving singularities in the correct manner. A numerical method specially designed to resolve the dynamics of moving singularities arising in the solution of nonlinear partial differential equations which exhibit finite-time blow-up has been published by Weideman (2003). Therein, a combination of a conventional spectral method and numerical analytic continuation of the solution

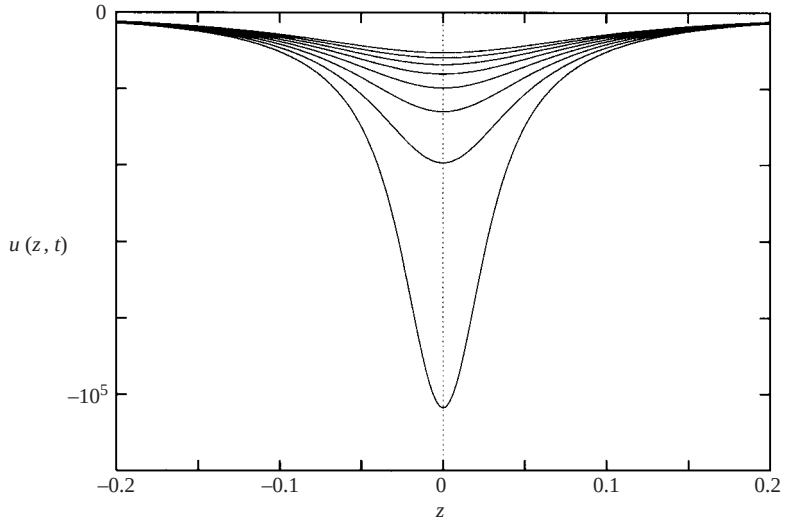

FIGURE 6. Numerical solution of (4.2) with forcing (4.7) before blow-up $t < t^*$ – the last eight time steps. Chosen parameters: $a = 30$, $\omega = 2$, $B = 0.1$, $L = 5$, $\Delta t = 10^{-5}$, $\Delta z = 10^{-3}$.

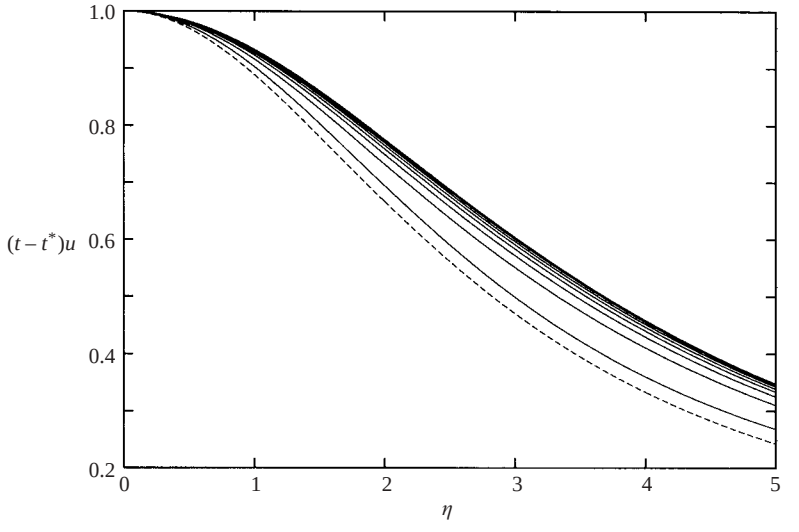

FIGURE 7. Numerical solution of (4.2) with forcing (4.7) approaching the blow-up profile f_0^-, (4.14) (dashed line), corresponding to figure 6 – the last eight successive time steps.

into the complex plane by means of Padé approximations is used to calculate the trajectories of singularities in the complex plane before blow-up. In the context of the present paper, one of the presented examples (heat equation with quadratic nonlinearity) is of special interest insofar as it exactly confirms our findings provided the symmetry relation (4.15) is taken into account.

4.2. *Finite-time blow-up: before and beyond*

Following the presentation of numerical evidence for the formation of finite-time singularities and the possibility of continuing the solutions of (4.2) beyond blow-up

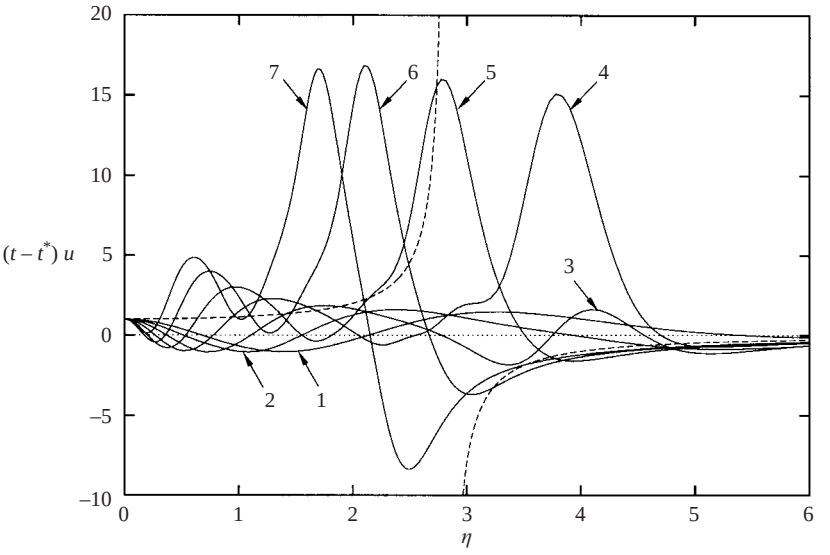

FIGURE 8. Numerical solution of (4.2) with forcing (4.7) beyond blow-up, $a=30, \omega=2$, $B=0.1, L=5,\ \Delta t=10^{-5}, \Delta z=10^{-3}$. Numbers indicate the number of successive time steps after the blow-up time $t^*\doteq 4.3359175$. Dashed line: blow-up profile f_0^+, (4.14).

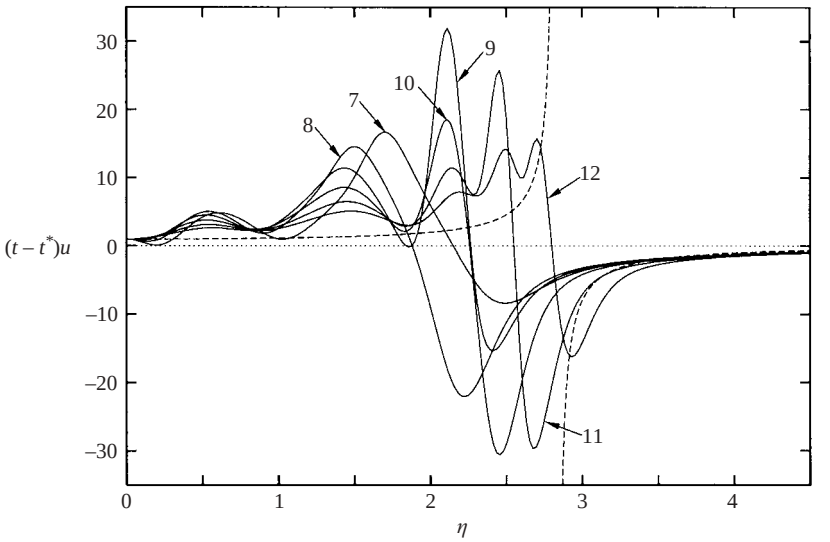

FIGURE 9. Numerical solution beyond blow-up (for legend see figure 8).

even in the case of three-dimensional flows, we next analyse this phenomenon using asymptotic methods.

Without loss of generality, we locate the finite-time blow-up at $t=t^*=0$ and for three-dimensional flow additionally at $z=z^*=0$.

For planar flow, the behaviour of the solution near the blow-up point is simply given by

$$u(t) \sim \frac{1}{t}+\frac{1}{2}+\frac{1+4g(0)}{12}\,t+\frac{g'(0)}{4}\,t^2+O(t^3), \quad t\to 0^{\pm}, \tag{4.8}$$

and therefore confirms the observed pole-like singularity in the numerical solution and its continuation beyond the blow-up time (figure 5).

In the case of three-dimensional flow, the asymptotic analysis of the flow structure near blow-up is significantly more complicated owing to a subtle balance between the time-dependent, nonlinear and diffusion terms of (4.2) and is not fully understood yet. Here, we follow the investigation of an evolution equation with cubic nonlinearity by Hocking *et al.* (1972). The 'approximate similarity' ansatz proposed therein can readily be adopted to the form of (4.2) and yields the representation

$$u(z,t) \sim \frac{1}{t} f(\eta,\tau) + \cdots, \quad \eta = \frac{z}{\sqrt{|t|\,\tau}}, \quad \tau = -\ln|t| \to \infty, \tag{4.9}$$

which results in

$$f + \frac{\eta}{2} f_\eta - f^2 = \frac{\eta}{2\tau} f_\eta - f_\tau - \frac{\mathrm{sgn}(t)}{\tau} f_{\eta\eta} - \mathrm{sgn}(t)\,\mathrm{e}^{-\tau} f - \mathrm{e}^{-2\tau} g. \tag{4.10}$$

In the immediate vicinity of the blow-up point, the linear and the forcing term of the right-hand side of (4.2) play an insignificant role since they are exponentially small in the representation (4.10) and therefore neglected in the further investigation.

The appropriate coordinate expansion of f is

$$f(\eta,\tau) \sim f_0(\eta) + g_1(\eta)\frac{\ln\tau}{\tau} + \frac{f_1(\eta)}{\tau} + O\left(\frac{\ln^2\tau}{\tau^2}\right), \tag{4.11}$$

leading to the system of first-order ordinary differential equations

$$f_0 + \frac{\eta}{2} f_0' - f_0^2 = 0, \quad f_n + \frac{\eta}{2} f_n' - 2 f_0 f_n = G_n, \quad g_n + \frac{\eta}{2} g_n' - 2 f_0 g_n = H_n, \tag{4.12a–c}$$

with $n = 1, 2, \ldots$ where $G_n(\eta), H_n(\eta)$ are functionals of $f_0, f_1, \ldots, f_{n-1}$ and $g_1, \ldots, g_{n-1}$. To ensure uniformly valid expansions for $\eta \to 0$, i.e. avoid the appearance of logarithmic singularities at the axis $\eta = 0$, the condition

$$G_n''(0) - \frac{\mathrm{sgn}(t)}{2} G_n(0) = 0 \tag{4.13}$$

for the right-hand side of (4.12*b*) must be satisfied (Hocking *et al.* 1972). The results for the coefficient functions of (4.11), taking into account (4.13), are given by

$$f_0^{\mp} = \frac{8}{8 \pm \eta^2}, \quad g_1^{\mp} = \mp\frac{10\,\eta^2}{(8 \pm \eta^2)^2}, \quad f_1^{\mp} = \frac{16 \mp c_1\eta^2 \mp 8\eta^2 \ln|8 \pm \eta^2|}{(8 \pm \eta^2)^2}, \tag{4.14}$$

where c_1 is an arbitrary constant depending on initial conditions and the upper/lower sign corresponds to $t \to 0^{\mp}$. It should be noted that the form of the results (4.14) associated with these limits reflects the remarkable transformation property of (4.10) with exponentially small terms being dropped

$$u(z,t) = -u(\mathrm{i}z, -t) \to f(\eta,\tau;t) = f(\mathrm{i}\eta,\tau;-t), \tag{4.15}$$

which shows that the flow behaviour for $t \to 0^+$ can be derived directly from the flow behaviour for $t \to 0^-$ by the simple change $\eta^2 \to -\eta^2$ of variables. Physically, this means that the focusing of the blow-up profile gives birth to two singularities located at $\eta = \pm\sqrt{8}$ which move away from the line of symmetry $z = 0$ in opposite directions. Further insight into this process may be gained from figure 10 which displays the functions $f_0(\eta)$, $g_1(\eta)$ entering the leading-order terms of the representation (4.11) for $f(\eta,\tau)$.

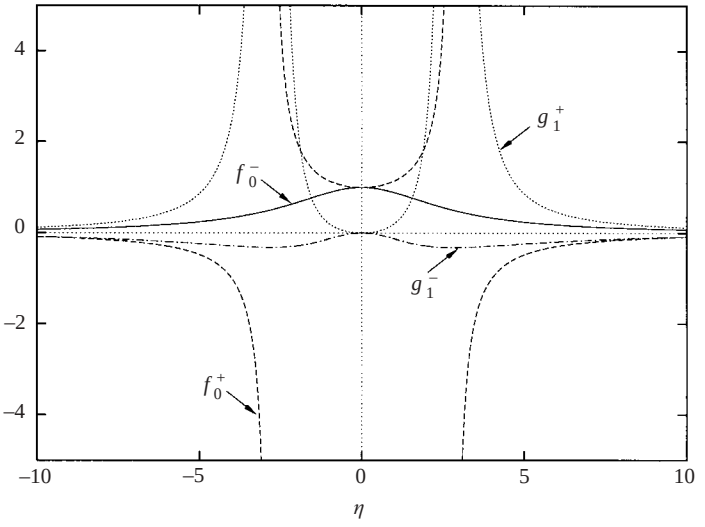

FIGURE 10. First- and second-order spatial structure of finite-time blow-up, equation (4.14).

A comparison between the leading-order blow-up profiles $f_0^{\pm}(\eta)$ and numerical calculations is given in figures 7 to 9. For $t<0$, the agreement between numerical and asymptotic results is almost perfect. Larger discrepancies, however, are observed for $t>0$. These are expected to result primarily from shortcomings of the numerical scheme which is able to capture the correct decay behaviour for $\eta \to \pm\infty$, but fails to resolve adequately the pole-like singularities occurring in the solution. Despite these difficulties, the qualitative agreement between numerical and analytical results clearly adds further support to the theoretical prediction of moving singularities emerging beyond blow-up. The result

$$u(z,t) = \left(t + \frac{z^2}{8\ln|t|} + \cdots \right)^{-1}, \quad t \to 0^{\pm}, \tag{4.16}$$

following from (4.9) and (4.14) shows that the blow-up or bursting process represents a localized phenomenon. The numerical results for $t>0$ reflect the internal structure of the moving singularity where – as discussed later – expansion (4.11) fails to yield a uniformly valid description of the solution near these singularities and therefore does not really fit to the predicted pole of first order with the exception of the decay behaviour for $\eta \to \pm\infty$.

As pointed out before, (4.15) has the important consequence that the solutions holding before and after blow-up are related via a simple change of coordinates. However, while the asymptotic representation for f^- is uniformly valid in the sense that higher-order terms produce small corrections to the lower-order terms everywhere, this is no longer the case for f^+. In fact, it is easily seen that all terms are of equal magnitude in the vicinity of the moving singularities where $\eta^2 - 8 \sim O(\ln\tau/\tau)$. To restore uniform validity of the solution for times beyond blow-up, an attempt was made to consider the neighbourhood of the moving singularities separately. From the inspection of (4.10), it is clear that the effect of diffusion first enters the expansion (4.11) at the level of $O(1/\tau)$. In the immediate neighbourhood of the singularities where large gradients exist, a balance between transient, nonlinear and diffusion terms

is expected. This in turn suggests the introduction of the stretched inner variable

$$y = (\eta - \sqrt{8})\tau, \tag{4.17}$$

(here for the right running singularity $\eta \to \sqrt{8}$) to obtain from (4.10)

$$\sqrt{2}\tau F_y - F^2 + \tau F_{yy} = -F - \frac{y}{2}F_y - \frac{y}{2\tau}F_y + \sqrt{2}F_y - F_\tau + O\left(\mathrm{e}^{-\tau}\right) \tag{4.18}$$

with $F(y, \tau) = f(\eta, \tau)$. The corresponding inner expansion is

$$F(y, \tau) \sim \tau F_0(y) + F_1(y) + \frac{F_2(y)}{\tau} + O(\tau^{-2}), \tag{4.19}$$

leading to the staggered system

$$\sqrt{2}F_0' - F_0^2 + F_0'' = 0, \tag{4.20a}$$

$$\sqrt{2}F_1' - 2F_0F_1 + F_1'' = -F_0 - \frac{y - \sqrt{8}}{2}F_0', \tag{4.20b}$$

$$\sqrt{2}F_2' - 2F_0F_2 + F_2'' = -F_0 - \frac{y}{2}F_0' - F_1 + F_1^2 - \frac{y - \sqrt{8}}{2}F_1', \cdots. \tag{4.20c}$$

According to (4.20*a*), the internal structure of the moving singularity is essentially a pole of second order $F_0 \sim 6/(y - y_s)^2$ located at $y = y_s$ which decays in the form $F_0 \sim -\sqrt{2}/y$ as $y \to \pm\infty$.

To match inner and outer solution, the corresponding expansions for $y \to \pm\infty$ and $\eta - \sqrt{8} \to 0$ are compared,

$$\left.\begin{aligned} F_0 &\sim -\frac{\sqrt{2}}{y} + \frac{2\ln|y|}{y^2} + \frac{C_0}{y^2} + O\left(\frac{\ln^2|y|}{y^3}\right), \\ F_1 &\sim \frac{1}{4} + \frac{\ln|y|}{\sqrt{2}y} + \cdots, \quad F_2 \sim -\frac{y}{16\sqrt{2}} + \cdots, \end{aligned}\right\} \tag{4.21}$$

$$\left.\begin{aligned} f_0^+ &\sim -\frac{\sqrt{2}}{\eta - \sqrt{8}} + \frac{1}{4} - \frac{\eta - \sqrt{8}}{16\sqrt{2}} + \cdots, \\ g_1^+ &\sim \frac{5}{2(\eta - \sqrt{8})^2} + \frac{5}{4\sqrt{2}(\eta - \sqrt{8})} + \cdots, \\ f_1^+ &\sim \frac{2 + c_1 + 8\ln(2\sqrt{8}) + 8\ln|\eta - \sqrt{8}|}{4(\eta - \sqrt{8})^2} + \cdots. \end{aligned}\right\} \tag{4.22}$$

As we can see, f_0^+ matches the leading-order terms of F_0, F_1 and F_2, whereas terms of $O(\ln\tau/\tau)$ differ by a factor of 1/2. Terms of $O(1/\tau)$ can be matched provided that $C_0 = 2 + c_1 + 8\ln(2\sqrt{8})$. This matching discrepancy apparently arises from the gap between the region of breakdown of the outer expansion (4.11) and the extension of the internal structure of the moving singularities. Since it is not clear how to overcome this difficulty at present, a close investigation of the flow behaviour near the singularities if desired has probably to resort to the numerical solution of the full equation (4.2). In this connection, the following observation may be important. The asymptotic representation of f^- involves an infinite number of arbitrary constants which allows the embedding of the local into a global solution. Because of the uniform validity of this expansion, however, constants entering at higher order have an increasingly weaker effect on the result. Obviously, this is no longer true for

$t > 0$ where all these constants are of equal importance in the neighbourhood of the moving singularities where (4.11) fails to yield a uniformly valid expansion. This in turn may suggest that the solution there depends strongly on weak changes of initial conditions before blow-up, possibly associated with chaotic behaviour. Clearly, further investigations are required to clarify this important issue.

Inspection of (4.14) reveals an obvious weakness of the expansion (4.11), that the location of the moving singularities is fixed at $\eta_s = \pm\sqrt{8}$ to all orders and thus does not allow for corrections of the paths as the number of terms is increased. More flexibility in this respect can be gained by applying the method of strained coordinates to (4.11) which is found to be equivalent with an alternative and inverse formulation of (4.9):

$$u(z,t) \sim \frac{1}{t}\frac{1}{h(\eta,\tau)} + \cdots, \quad h(\eta,\tau) = h_0(\eta) + j_1(\eta)\frac{\ln\tau}{\tau} + \frac{h_1(\eta)}{\tau} + \cdots. \tag{4.23}$$

In this context, we refer to the study by Velázquez, Galaktionov & Herrero (1991) who used this inverse formulation and (in contrast to the approach by Hocking *et al.* 1972) the method of matched asymptotic expansions to obtain the expansion (4.23). Unfortunately, however, the result

$$h^{\pm}(\eta,\tau) \sim 1 \mp \frac{\eta^2}{8} \mp \frac{5\eta^2}{32}\frac{\ln\tau}{\tau} - \left(\frac{1}{4} \pm c_1\eta^2 \pm \frac{\eta^2}{8}\ln|\eta^2 \mp 8|\right)\frac{1}{\tau} + \cdots \tag{4.24}$$

loses its uniform validity in the same η, τ domain as expansion (4.11), but it is not clear anyway if the concept of uniform validity can be maintained because of the presence of singularities. Since the paths of the moving singularities are determined by the zeros of $h^+(\eta,\tau)$ it, nevertheless, indicates more clearly that $\eta_s(\tau)$ may deviate from the values $\pm\sqrt{8}$ by corrections of $O(\ln\tau/\tau)$:

$$\eta_s(\tau) = \frac{z_s(t)}{\sqrt{t\tau}} = \pm\sqrt{8} + O(\ln\tau/\tau). \tag{4.25}$$

As shown in figure 11, this is also supported by the numerical results of the numerical test case discussed in § 4.1 which can be represented reasonably accurately by the curve fit $\eta_s(\tau) = \pm(\sqrt{8} + 2.664\ln\tau/\tau)$.

4.3. *Singular travelling waves*

It is well known that Fisher's equation (4.2) admits bounded solutions which describe waves of constant form travelling in the lateral direction (see e.g. Sherratt 1998 and references therein). Here, we are concerned with the occurrence of singular travelling waves. If u is written in the form

$$u(z,t) = \bar{u}(\xi), \quad \xi = z - Ut - \xi_0, \tag{4.26}$$

where ξ and U denote the wave coordinate and the wave speed and the arbitrary constant ξ_0 accounts for the translation invariance of the wave profile, (4.2) without the forcing term reduces to

$$\bar{u}'' + U\bar{u}' + \bar{u} - \bar{u}^2 = 0. \tag{4.27}$$

Because of the invariance property $u(z,t;-U) = u(-z,t;U)$, it is sufficient to consider right running waves only. Bounded solutions join the stationary states $\bar{u} = 1$ and $\bar{u} = 0$, whereas the (single, isolated) singular solutions deviate from and return to the stable

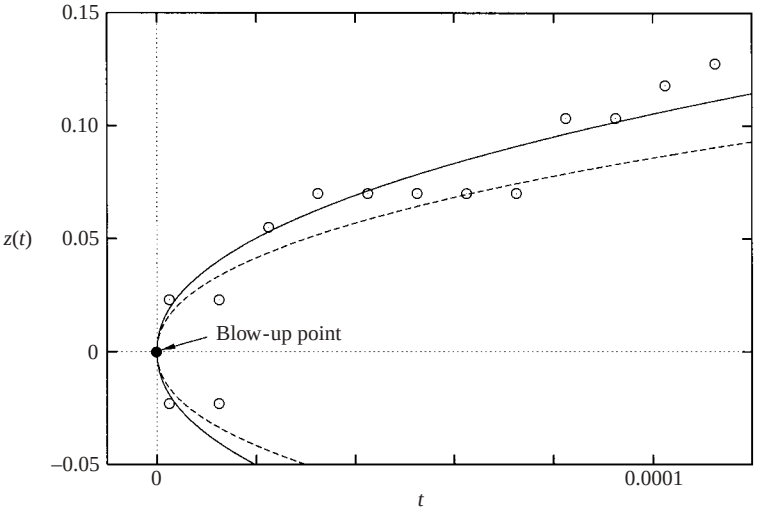

FIGURE 11. Generation of a pair of moving singularities: asymptotic versus numerical results. Path of singularity $\eta_s(\tau)$ – open circles denote location of 'singularities', i.e. the maxima of the curves in figures 8 and 9, solid line: least-squares fit $\eta_s = \pm(\sqrt{8} + 2.664 \ln \tau/\tau)$, dashed line: leading-order asymptotic result $\eta_s = \pm\sqrt{8}$, (4.25).

upper-branch level $\bar{u} = 1$ having the decay behaviour

$$\bar{u}(\xi) \sim 1 \mp a \exp\left[-\left(\frac{U}{2} \pm \sqrt{\frac{U^2}{4} + 1} \right) \xi \right], \quad a \ll 1 \tag{4.28}$$

as $\xi \to \pm\infty$ and the structure

$$\bar{u}(\xi) \sim \frac{6}{(\xi - \xi_s)^2} - \frac{6U}{5(\xi - \xi_s)} + \frac{25 - U^2}{50} + O(\xi - \xi_s), \quad \xi \to \xi_s \tag{4.29}$$

near the pole where ξ_s denotes the location of the singularity. Representative examples are shown in figure 12. The limiting behaviour of (4.27) for $U \to \infty$ can be obtained by the transformation $\bar{u}(\xi) = U^2 \phi(\zeta)$, $\xi = \zeta/U$, yielding

$$\phi' - \phi^2 + \phi'' \sim O(U^{-2}), \tag{4.30}$$

which is of the form of equation (4.20*a*). The internal structure of the moving singularities just beyond blow-up therefore can be interpreted as singular travelling waves in the limit of large wave speeds. On the other hand, the solution corresponding to the stationary limit $U = 0$ is given by

$$\bar{u}(\xi) = 1 + \tfrac{3}{2} \sinh^{-2}\left(\frac{\xi}{2} \right), \tag{4.31}$$

which is the aperiodic limiting case (with the invariant $g_3 = -1/216$) of the general solution containing the Weierstrass elliptic $\wp$-function (Abramowitz & Stegun 1970)

$$\bar{u}(\xi) = 6\wp\left(\xi ; \tfrac{1}{12}, g_3 \right) + \tfrac{1}{2}. \tag{4.32}$$

The absence of any forcing term enables the specification of the closed-form solution (4.32) describing a periodic array of singularities which also indicates the infinite number of possible solutions reflected in the indeterminacy of g_3.

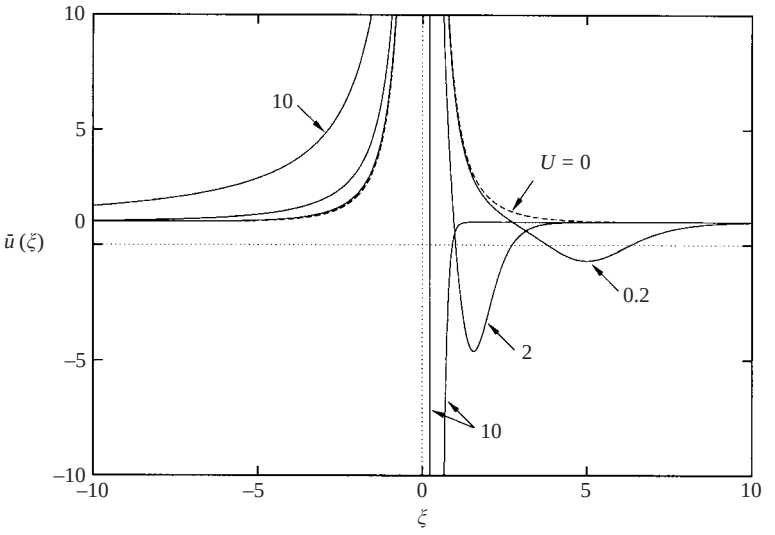

FIGURE 12. Isolated singular travelling-wave solutions of Fisher's equation (4.27) for different values of the wave speed U and the choice $\xi_s = 0$ (right running wave). Dashed line: steady limit $U = 0$, equation (4.31).

4.4. *The supercritical flow regime* $\Gamma > \Gamma_c$

Note that the bifurcation structure outlined in § 3 is preserved for values of Γ beyond Γ_c with the exception of the sign in front of δ in (3.9) leading in turn to solutions c with complex stationary points $\pm \mathrm{i}c_s$. For this reason, no stationary states can be obtained in the case of $\Gamma > \Gamma_c$. Using the transformation of variables (4.1), we obtain the counterpart of (4.2),

$$\frac{\partial u}{\partial t} - \frac{\partial^2 u}{\partial z^2} = u - u^2 - \tfrac{1}{2} + g. \tag{4.33}$$

The essential feature of this equation becomes apparent if, similar to the subcritical case treated in § 4, the simple case of unforced planar flow with the initial condition $u(t_0) = u_0$ is considered. The resulting solution,

$$u(t) = \frac{u_0 + (u_0 - 1)\tan[(t - t_0)/2]}{1 + (2u_0 - 1)\tan[(t - t_0)/2]}, \tag{4.34}$$

now blows up in finite time whichever u_0 is chosen. However, also in this case, the solution can be continued beyond blow-up but, contrary to (4.3), bursts periodically with the cycle duration 2π (in the original time variable T, the period between successive bursts is $\pi/(\mu c_s \sqrt{\Gamma - \Gamma_c})$ and therefore tends to infinity as $\Gamma \to \Gamma_c$). This supercritical solution for unforced two-dimensional flow corresponds to the numerical results of Smith (1982), at least qualitatively, since $\Gamma - \Gamma_c$ there was chosen to be of $O(1)$ and not small as assumed here.

Finally, we briefly note that the local blow-up behaviour of three-dimensional flow described by (4.33) is identical to that investigated in § 4.2.

5. Flow control

Modern developments in aircraft design increasingly include applications of smart structures for flow control, i.e. a combination of sensors, actuators, real-time control

systems and data processing as well as the use of new materials to increase manoeuvrability, reduce drag and flow-induced noise radiation. Since leading-edge separation bubble bursting is associated with the rapid transition to turbulent boundary-layer flow and consequently with an increase of drag, it is desirable to retard the onset of separation bubbles.

The investigations carried out so far indicate that near critical flows where $\Gamma \approx \Gamma_c$ respond very sensitively to imposed disturbances such as inhomogeneities in the oncoming flow, external sound fields, structure vibrations and surface impurities due to icing, wetting and particle deposition. This sensitivity allows also for a very effective improvement or selective manipulation of the flow conditions in the crucial region of interaction by means of localized surface-mounted obstacles and/or suction/blowing distributions as outlined below.

5.1. *Increase of the maximum angle of attack*

To motivate the effort to increase the value of Γ_c up to which steady states may exist, we draw attention to the results of a comparative study between Navier–Stokes computations and the interactive approach of marginal separation applied to a specific example of the planar steady flow past a thin symmetric airfoil at small angles of attack and the moderate Reynolds number of 20 000 (Braun *et al.* 2003). The breakdown of classical boundary-layer theory in the form of the marginal separation singularity occurred at an angle α_c of approximately 3.37°, whereas the Navier–Stokes computations and the interaction theory admit converged solutions up to the coincident values $\alpha_m \approx 4.25°$ and 4.44°, respectively. The unexpected large difference of about one degree between the breakdown of the classical boundary-layer calculation and that of the interaction theory corresponding to $(\alpha_m - \alpha_c) \propto Re^{-2/5}\Gamma_c$ clearly indicates that mechanical devices which allow Γ_c to increase may prove efficient in achieving substantially higher maximum lift without bubble bursting.

From (3.6), it is seen that the value of Γ_c can be affected by planar obstacles and suction distributions. In the following, we concentrate on two examples, an obstacle shape with continuous curvature and a suction slot with a constant suction rate. Specifically, we consider the family of obstacles

$$h_\infty(X) = H\left[1 - \left(\frac{2(X - X_c)}{L}\right)^2\right]^3 \theta\left(\frac{L}{2} - |X - X_c|\right) \tag{5.1}$$

and suction distributions

$$v_{w\infty}(X) = V\theta\left(\frac{L}{2} - |X - X_c|\right), \tag{5.2}$$

where the parameters X_c, L, H and V denote the location, length of the device, height of the obstacle and the suction rate, as indicated also in figures 18 and 19.

In the first example, the parameters H or alternatively V were varied for a fixed location $X_c = 0$ and a set of different values of the length of the device. For each parameter combination the value of Γ_c was determined by means of the numerical procedure described in Braun & Kluwick (2002*a*). The results depicted in figures 13 and 14 show that the value $\Gamma_c \approx 2.66$ associated with the case of $H = V = 0$ can be exceeded significantly if we choose H to be positive (corresponding to a hill), V to be negative (which means suction) and L as large as possible. In contrast, dents and blowing are seen to lead to a reduction of Γ_c. Note that the characteristic shape of the limiting curves $\Gamma_c = \Gamma_c(L, H)$ indicates the existence of optimal parameter combinations (L, H) for which Γ_c is a maximum. Computed leading-order wall shear

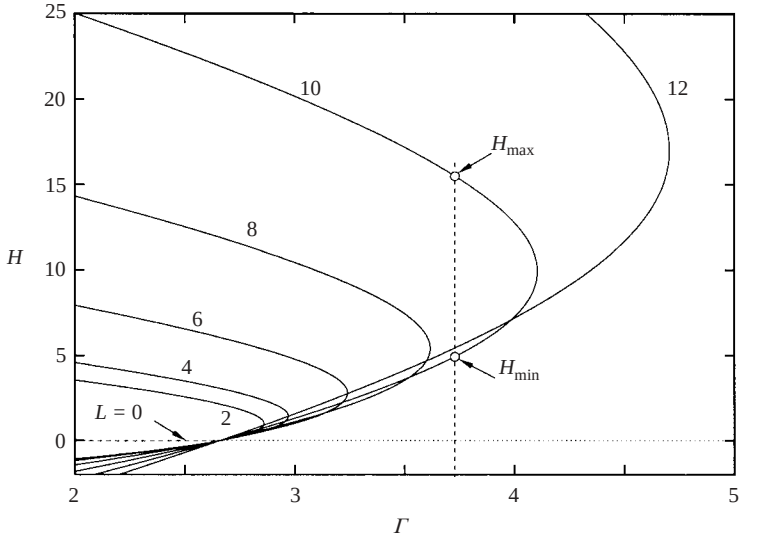

FIGURE 13. Extension of Γ in the case of the planar-flow problem by means of a surface-mounted obstacle according to (5.1) with $X_c = 0$. Solutions of (2.9) for a given Γ and L exist in the range of $H \in [H_{\min}, H_{\max}]$ in the left-hand side domain of the drawn limiting curves $\Gamma = \Gamma_c$.

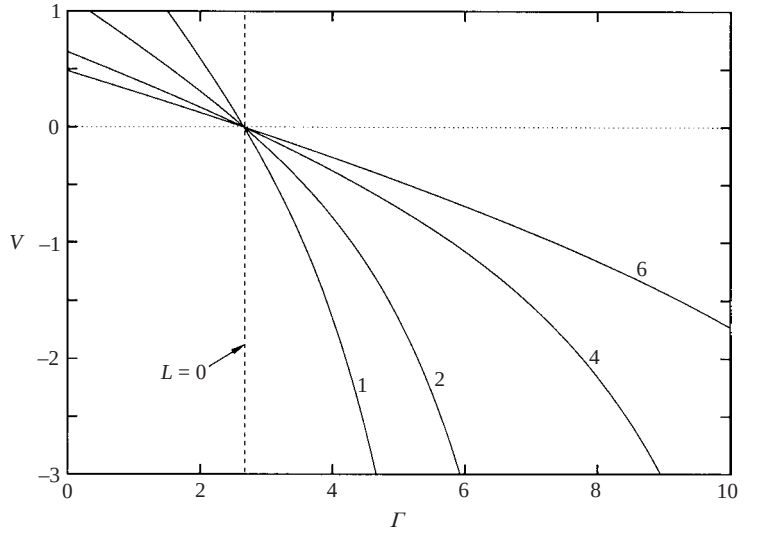

FIGURE 14. Extension of Γ in the case of the planar-flow problem by means of a suction distribution according to (5.2) with $X_c = 0$. Solutions for a given Γ and L exist in the left-hand side domain of the drawn limiting curves $\Gamma = \Gamma_c$.

distributions $A_{\infty c}(X)$ and right eigenfunctions $b(X)$ for different values of V and $L = 4$ are depicted in figures 15 and 16.

In the second example, the location X_c of the devices is shifted along the X-axis and the parameters H, V and L are held constant (figures 17 and 18). Of course,

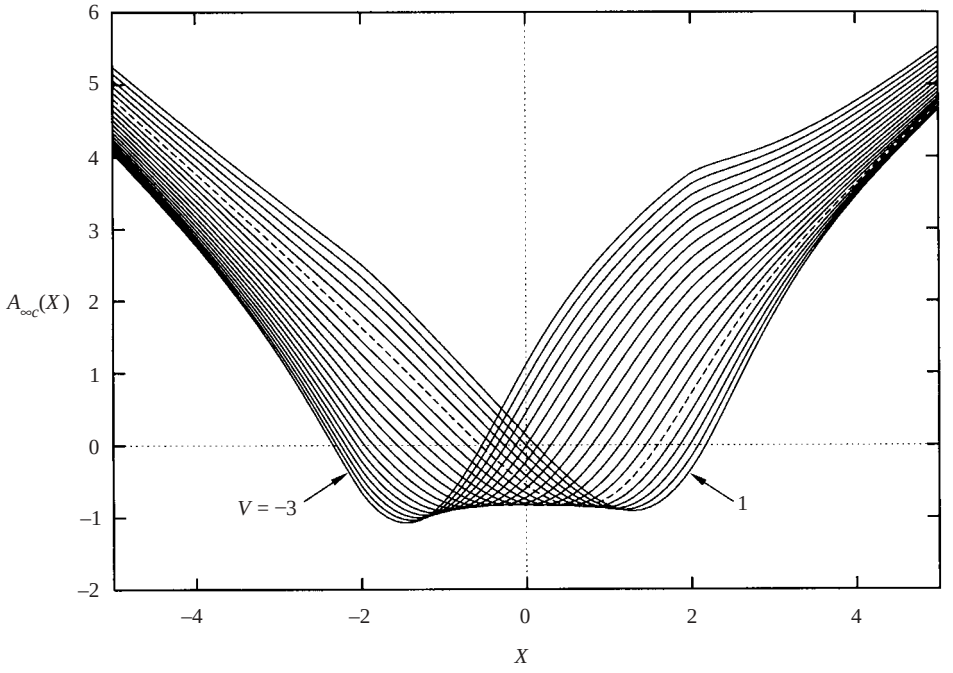

FIGURE 15. Solutions of (3.6) for a suction distribution according to (5.2) with $X_c = 0$, $L = 4$ and $h_\infty = 0$ in dependence of the amplitude $V \in [-3, 1]$ (steps $\Delta V = 0.2$). Dashed line: $A_{\infty c}(X)$ for $v_{w\infty} = h_\infty = 0$.

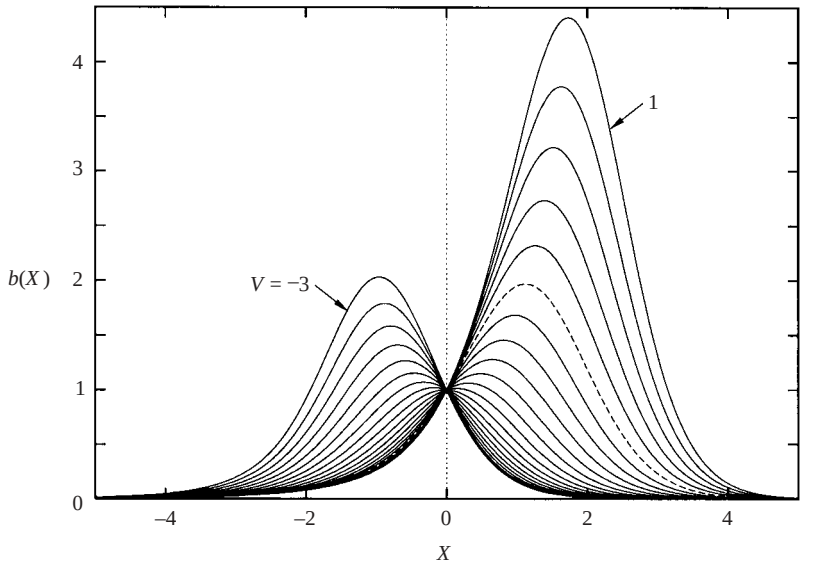

FIGURE 16. Solutions of (3.7) for a suction distribution according to (5.2) with $X_c = 0$, $L = 4$ and $h_\infty = 0$ in dependence of the amplitude $V \in [-3, 1]$ (steps $\Delta V = 0.2$). Dashed line: $b(X)$ for $v_{w\infty} = h_\infty = 0$.

the influence of these devices on Γ_c tends to zero as $X_c \to \pm\infty$ (i.e. when their effect on the interaction process becomes less important and eventually vanishes) and the value $\Gamma_c \approx 2.66$ is reached in these limits. As we can see, the location of the obstacle

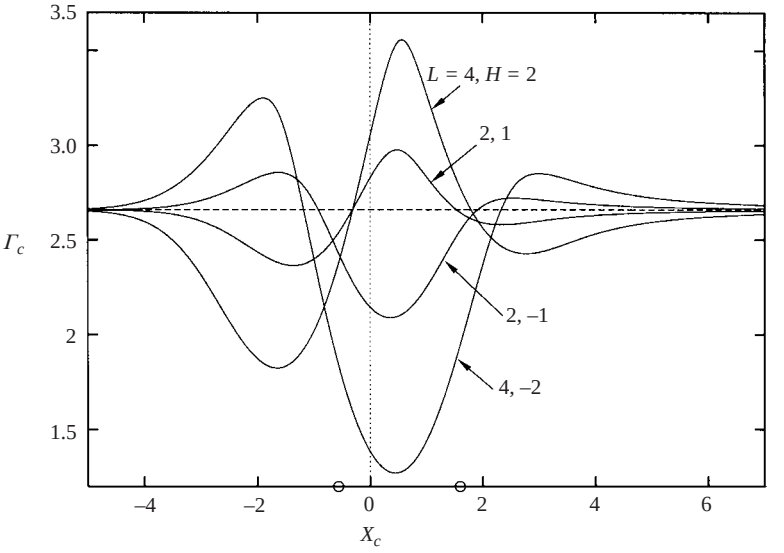

FIGURE 17. Maximum possible angle of attack Γ_c for the solution of (3.6) with $v_{w\infty} = 0$ in dependence of location X_c and shape parameters L and H of an obstacle according to (5.1). Dashed line: $\Gamma_c \approx 2.66$ for $H = 0$; open circles denote leading-order separation and reattachment position for $H = 0$.

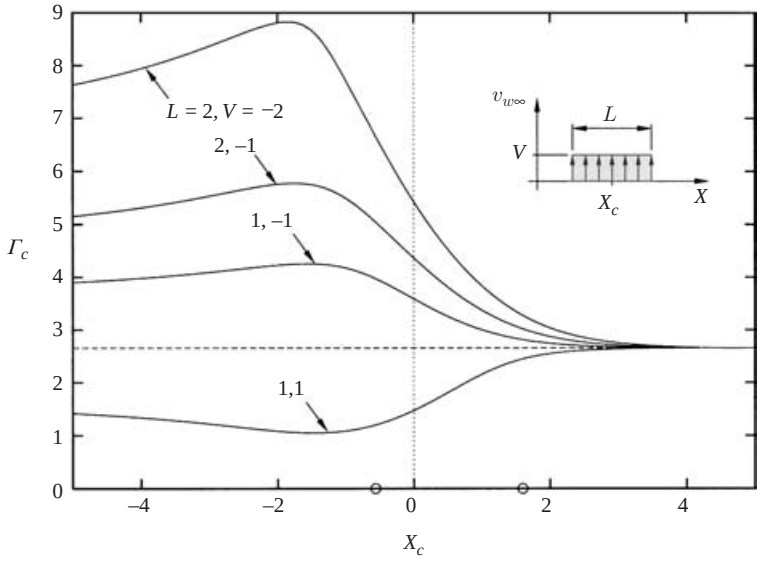

FIGURE 18. Maximum possible angle of attack Γ_c for the solution of (3.6) with $h_\infty = 0$ in dependence of location X_c and shape parameters L and V of a suction distribution according to (5.2). Dashed line: $\Gamma_c \approx 2.66$ for $V = 0$; open circles denote leading-order separation and reattachment position for $V = 0$.

affects Γ_c very sensitively. In the case of the suction distribution, however, the value of Γ_c is less sensitive with respect to the centre location if $X_c < 0$; its effect decays very slowly.

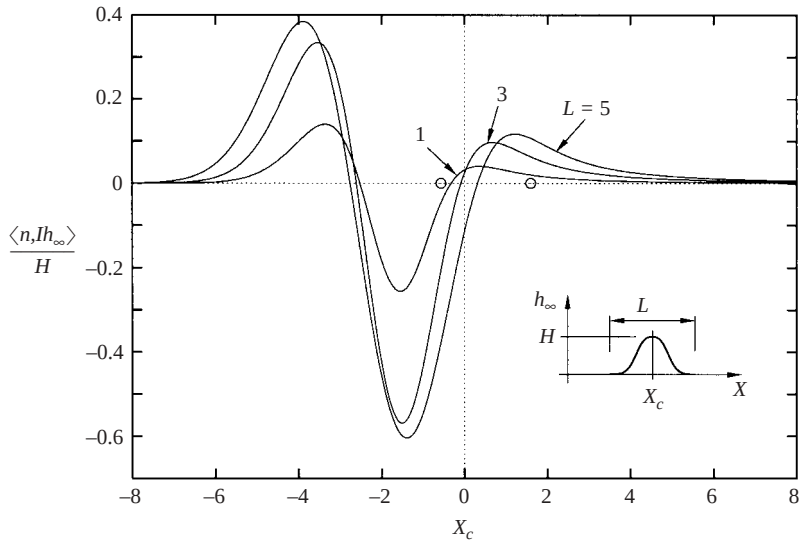

FIGURE 19. Forcing amplitude in dependence of location X_c and length L of an obstacle according to (5.1). Open circles denote leading-order separation and reattachment positions.

For practical purposes, consider again the flow around the airfoil at a Reynolds number of 20 000 mentioned above. In this special case, $L = 1$ and $H = 1$ corresponds to 3.2% and 0.1% of the chord length $\bar{L}$, respectively, and $V = 1$ to 0.86% of the free-stream velocity $\bar{u}_\infty$.

5.2. *Forcing amplitude*

We conclude this section with the calculation of the forcing amplitude of the term $\bar{g}$ given by the scalar products (3.10) using just (5.1) and (5.2) for the X-dependence of the three-dimensional unsteady disturbances h_1 and v_{w1}, respectively. Further, we assume vanishing $O(1)$ contributions to h and v in (3.3), i.e. write $h = \varepsilon^4 h_\infty(X) h^*(\bar{Z}, \bar{T})$ and $v = \varepsilon^4 v_{w\infty}(X) v^*(\bar{Z}, \bar{T})$ with unspecified functions h^*, v^*. Results depending on the location X_c and the length of the devices are shown in figures 19 and 20. The location of the surface-mounted obstacle is much more sensitive concerning the amplitude than that of the suction distribution. In both cases, their effect can be maximized if they are placed immediately upstream of the separation bubble. An efficient method for increasing the forcing amplitude is to increase the curvature of the obstacle, as can be seen by inspecting the form of the integral operator I, (3.5). This fact appears to be intuitively realized in the application of sharp-edged zigzag tape turbulators in the nose region of airfoils.

6. Summary and conclusions

Analytical and numerical methods were used to study the response of a steady two-dimensional marginally separated boundary layer to unsteady three-dimensional disturbances in the limit $\Gamma_c - \Gamma \to 0$. Specifically, it was shown that the perturbations of the wall shear stress can there be written as a product containing two functions b and u depending on the streamwise direction X and, respectively, the lateral distance $z \propto |\Gamma_c - \Gamma|^{1/4} Z$ and time $t \propto |\Gamma_c - \Gamma|^{1/2} T$ only. Furthermore, it was shown that $b(X)$ is fully determined by the properties of the undisturbed flow for $\Gamma = \Gamma_c$ with the important consequence that the response of the boundary layer in terms

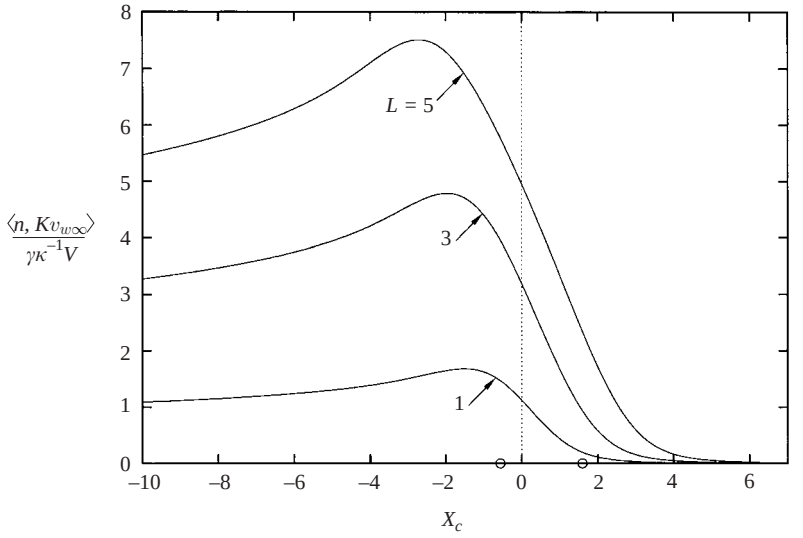

FIGURE 20. Forcing amplitude in dependence of location X_c and length L of a suction distribution according to (5.2). Open circles denote leading-order separation and reattachment positions.

of the streamwise distance is the same for all possible unsteady three-dimensional disturbances. The second contribution to the perturbation wall shear stress $u(z, t)$ which accounts for its variation in the lateral direction and with time was found to be governed by a nonlinear diffusion equation of the Fisher type. If the flow disturbances are taken to be independent of z, this equation reduces to an ordinary differential equation which admits analytical solutions if there is no external forcing due to surface-mounted obstacles or suction devices. In the below-critical regime $\Gamma < \Gamma_c$, there exist two stationary points $u = (1, 0)$ characterizing the upper- and lower-branch solutions associated with the unperturbed flow which are seen to be attracting and repelling, respectively. Wall shear stress distributions, therefore, remain smooth for all times if the initial value $u(0) > 0$. In contrast, solutions starting with $u(0) < 0$ exhibit finite-time blow-up $u \to -\infty$ for $t \to t^* < \infty$. Most important, however, the occurrence of this singularity does not terminate the solution which can be continued beyond blow-up and approaches the upper branch eventually as $t \to \infty$.

No stationary points exist in the above-critical regime $\Gamma > \Gamma_c$ and finite-time blow-up is found to be inevitable. As in the below critical regime, solutions can be continued beyond the blow-up time t^*. However, since a steady unperturbed state does not exist for $\Gamma > \Gamma_c$, the disturbances cannot consolidate, but blow up again in finite time. This eventually leads to a time periodic flow pattern which describes self-sustained oscillations of the separation bubble including repeated bubble bursts. The associated time period $\Delta\bar{t}^*$ is independent of the initially imposed disturbance level and most conveniently expressed in terms of the Strouhal number

$$Str = \frac{\bar{L}}{\bar{u}_\infty \Delta\bar{t}^*} \sim \frac{a_0^{9/10} U_{00}^{1/5} \mu c_s (\Gamma - \Gamma_c)^{1/2}}{p_{00}^{3/10} \pi Re^{1/20}} + \cdots \tag{6.1}$$

as $\Gamma - \Gamma_c \to 0^+$ and $Re \to \infty$.

No analytical solutions of the Fisher equation are known if the wall shear stress distribution depends on the lateral distance. Numerical experiments have shown,

however, that singularity formation is possible also in this case both in the below-critical and above-critical regimes. Asymptotic analysis indicates that the blow-up phenomenon is local in the sense that it occurs at a finite spatial position, at a finite time. Moreover, as in strictly two-dimensional flows, the solution can be continued beyond blow-up thereby giving rise to the formation of moving singularities. These represent propagating vortex sheets qualitatively similar to Λ-vortices arising in the early stages of laminar–turbulent transition in short separation bubbles.

In addition to unsteady flows, steady strictly two-dimensional flows have also been investigated with special emphasis on the effect of surface-mounted obstacles and/or suction. It was found that the critical value Γ_c of the controlling parameter can be affected significantly by such devices which might prove useful in practical applications.

Probably the most relevant study to which the predictions of the present paper regarding the late stages of laminar separated flow can be compared is that of Alam & Sandham (2000). They investigated a representative example of marginally separated flow with turbulent reattachment using direct numerical simulation of the incompressible Navier–Stokes equations. A steady planar Blasius boundary-layer-type flow was forced to separate over a short distance. Localized unsteady three-dimensional disturbances in the form of a suction strip were used to trigger the fast transition process to turbulent boundary-layer flow. Although it would be possible to perform a quantitative comparison (at least in principle) we just highlight some obvious analogies. Concerning two-dimensional flow, it was perceived that vortex shedding (which is seen to be confined to the boundary layer) persisted even without external forcing of the flow, 'though there is disagreement about a precise shedding criterion' due to parasitic disturbances of the inflow and outflow boundary conditions of the numerical scheme (Alam & Sandham, p. 25, figure 26 *a*, *b*). In the light of the present investigation, self-sustained vortex shedding in the form of oscillatory blow-up is clearly attributed to supercritical flow conditions, see, for example the similarity law (6.1). In the case of three-dimensional flow figure 11(*a*) (Alam & Sandham, p. 13) is of particular interest: periodic forcing results in coherent structures of the instantaneous contours of the streamwise velocity which eventually collapse, slowly recovering to an equilibrium turbulent boundary layer; individual bursts reflect the shape of the function $b(X)$ (cf. figure 16) well. Finally, the surface plot of spanwise vorticity (Alam & Sandham, figure 12(*b*), p. 14) displays Λ-shaped vortical structures within the mean separated region whose core resembles the path of the moving singularities calculated in § 4 (the spanwise vorticity ω_z is, apart from planar contributions, proportional to the product of $b(X)c(\bar{Z}, \bar{T})$, cf. (3.17)). Their interaction seems to be responsible for the generation of considerably smaller structures associated with the developing turbulent flow. In this connection, it should be noted that the (small) drifting speed of these structures in the streamwise direction within the framework of the present theory is an effect of higher order which has not been calculated so far. For a detailed comparison of the implications of the present theory to experimental observations concerning laminar/turbulent transition in separation bubbles, see Braun & Kluwick (2004).

Summarizing, the results obtained in the present study indicate:

(i) The passage through Γ_c is associated with a gradual rather than abrupt change of flow field. Finite-time singularities describing the phenomenon of bubble bursting may occur in below-critical as well as above-critical situations. However, while this phenomenon requires a certain finite perturbation level if $\Gamma < \Gamma_c$, it is triggered by even infinitesimally small disturbances if $\Gamma > \Gamma_c$ where also self-sustained oscillations

with periodically repeated bubble bursts are possible. Oscillating laminar separation bubbles have been calculated numerically by Hsiao & Pauley (1994) who observed that the associated amplitude of the reattachment line was significantly larger than that of the separation line. Within the framework of the present theory, this flow behaviour is captured by the eigenfunction $b(X)$ whose values at the reattachment and separation point differs by a factor of about 3.

(ii) The theory of marginally separated laminar flows can indeed describe phenomena which are of interest in the turbulence context. First, since finite-time blow-up appears to be a generic feature of above-critical flows 'the "spotty" or intermittent character of turbulent dissipation is immediately understandable in terms of the behaviour near points where singularities of vorticity (and the related deformation tensor) occur' (Moffatt 2001). Secondly, the structure of finite-time singularities clearly displays features which are reminiscent of early stages of laminar–turbulent transition,

(iii) Smart devices such as surface-mounted obstacles and/or suction stripes provide very effective means of increasing Γ_c, i.e. to delay laminar–turbulent transition.

Of course, a number of open problems remain. Probably the most important concerns the question if and how the finite-time singularities can be resolved by considering scales in space and time where the present theory loses its validity locally. As proposed in the study by Elliott & Smith (1987), an Euler stage is expected to come into play eventually where the vorticity generated near the wall penetrates into the outer part of the boundary-layer. Analytical and numerical evidence provided in the present study, however, indicates that singularities forming in the limit $|\Gamma - \Gamma_c| \to 0$ are much weaker than in cases where $|\Gamma - \Gamma_c| \sim O(1)$. As a consequence, it is expected that this process does not yet lead to a complete change of the flow field associated with the ejection of a vortex into the external potential flow field, but rather remains confined to the boundary thereby leading to a reduction of the velocity defect there which appears to be supported also by numerical findings reported in Alam & Sandham (2000), Braun *et al.* (2003) and Mary & Sagaut (2002).

The study of the dynamical behaviour of vortices and in particular the interaction of vortex sheets generated by different singularities represents an important task even in the framework of the present theory. As mentioned before, self-sustained oscillations with periodically occurring bubble bursts are possible in two-dimensional flows under above-critical conditions $\Gamma > \Gamma_c$. According to (6.1), the associated time period is fully determined by the properties of the unperturbed boundary layer for $\Gamma = \Gamma_c$, the difference $\Gamma - \Gamma_c$ and Re. Also, it was found possible to construct singular solutions describing three-dimensional steady flows which are periodic with respect to the distance in the spanwise direction where, however, the wavelength remains arbitrary, equation (4.32). It would thus be very important to investigate whether the forced Fisher equation (4.2) or its super-critical counterpart (4.33) admits in addition unsteady three-dimensional solutions describing bursting processes which are periodic in time and space and if a characteristic spanwise spacing of the singularities emerges from such an analysis. If so, this could shed some light on the streaky structure of transitional flows. In this connection, we also note the observation that the steady version of the Fisher equation agrees with the steady integrated version of the Korteweg–de Vries equation. The latter, however, is known to admit chaotic behaviour if periodically forced.

Multiplicity of solutions and critical values of the controlling parameter beyond which steady-state solutions do not exist are a characteristic feature of marginally separated flows. However, similar phenomena do occur also in situations where triple-deck theory applies, i.e. in situations where a fully attached boundary layer

is forced to separate owing to the presence of a large adverse pressure gradient. Examples displaying such a branching behaviour include supersonic flows past flared cylinders (Gittler & Kluwick 1987), subsonic flows past expansion ramps and subsonic trailing edge flows (Korolev 1990). Current work indicates that this indeed leads to phenomena similar to those described here. This observation is further supported by a recent publication of Borodulin *et al.* (2002) in which it was argued that bursting processes in transitional laminar boundary-layers share common universal properties that do not depend on the specific problem under consideration.

Finally, we note that the singularities arising in marginally separated flows are expected to be an effective source of acoustic noise which may be of interest in connection with flow control ('laminar–turbulent transition detection'). Again, this is an area of current work.

The authors are grateful to Professor A. I. Ruban for helpful comments and discussions, including in particular the ill-posedness of the Cauchy problem associated with the unsteady version of the interaction equation, during a visit to Vienna which was supported by the Austrian science foundation FWF in the context of the 'Wissenschaftskolleg Partielle Differentialgleichungen'.

Appendix. Calculation of higher-order contributions in the expansion of the wall shear

As pointed out in Braun & Kluwick (2003), it is necessary to apply Poincaré's method of strained coordinates for the spanwise direction to determine the higher-order contribution $d(\bar{T})$ in the expansion (3.4):

$$\varepsilon Z = \bar{Z} + \varepsilon^6 \ln \varepsilon \, \chi_1(\bar{Z}, \bar{T}) + \cdots . \tag{A 1}$$

If, as here, the investigation is restricted to symmetric functions h and v_w with respect to the spanwise coordinate resulting in $A(X, Z, T) = A(X, -Z, T)$, we obtain

$$d(\bar{T}) = \mathrm{e}^{-Q(\bar{T})} \left(d_0 + \int_{\bar{T}_0}^{\bar{T}} \mathrm{e}^{Q(t)} R(t) \, \mathrm{d}t \right), \tag{A 2}$$

with

$$\left.\begin{aligned} Q(\bar{T}) &= 2\mu \int_{\bar{T}_0}^{\bar{T}} c(0, t) \, \mathrm{d}t, \\ R(\bar{T}) &= \frac{\lambda}{8\pi \langle n, Kb \rangle} \frac{\partial^4 c}{\partial \bar{Z}^4}(0, \bar{T}) \left\langle n, \int_{-\infty}^{X} \frac{\mathrm{d}t}{\sqrt{X - t}} \int_{-\infty}^{\infty} (t - \xi) b \, \mathrm{d}\xi \right\rangle . \end{aligned}\right\} \tag{A 3}$$

Here, $d_0 = d(\bar{T}_0)$ and $\bar{T}_0$ denote a constant depending on the initial conditions and a reference time, respectively. The stretching function χ_1 is given by

$$\chi_1(\bar{Z}, \bar{T}) = \frac{1}{\langle n, I A_{\infty c} \rangle} \int_0^{\bar{Z}} \left[\langle n, b^2 \rangle \, d(\bar{T}) \, c(s, \bar{T}) \right.$$

$$\left. - \frac{\lambda}{16\pi} \left\langle n, \int_{-\infty}^{X} \frac{\mathrm{d}t}{\sqrt{X - t}} \int_{-\infty}^{\infty} (t - \xi) b \, \mathrm{d}\xi \right\rangle \frac{\partial^4 c(s, \bar{T})}{\partial s^4} \right] \mathrm{d}s + \frac{\langle n, Kb \rangle}{\langle n, I A_{\infty c} \rangle} d'(\bar{T}) \, \bar{Z}. \tag{A 4}$$

Numerical calculations for $h_\infty = v_{w\infty} = 0$ yield

$$\left\langle n, \int_{-\infty}^{X} \frac{\mathrm{d}t}{\sqrt{X-t}} \int_{-\infty}^{\infty} (t-\xi) b \, \mathrm{d}\xi \right\rangle \approx -132, \quad \langle n, I A_{\infty c} \rangle \approx 1.11. \tag{A 5}$$

In passing we note that the function d is absent in the case of strictly planar flow. The calculation of the term a_2 in the expansion (3.4) appears to be a sophisticated task which has not been carried out so far, see also the comments in Braun & Kluwick (2003).

REFERENCES

Abramowitz, M. & Stegun, I. A. 1970 *Handbook of Mathematical Functions,* 7th edn. Dover.

Alam, M. & Sandham, N. D. 2000 Direct numerical simulation of 'short' laminar separation bubbles with turbulent reattachment. *J. Fluid Mech.* **410**, 1–28.

Borodulin, V. I., Gaponenko, V. R., Kachanov, Y. S., Meyer, D. G. W., Rist, U., Lian, Q. X. & Lee, C. B. 2002 Late-stage transitional boundary-layer structures. Direct numerical simulation and experiment. *Theoret. Comput. Fluid Dyn.* **15**, 317–337.

Braun, S. & Kluwick, A. 2002*a* The effect of three-dimensional obstacles on marginally separated laminar boundary layer flows. *J. Fluid Mech.* **460**, 57–82.

Braun, S. & Kluwick, A. 2002*b* Unsteady three-dimensional effects in marginally separated laminar boundary layer flows. *AIAA Paper* 2002-2983.

Braun, S. & Kluwick, A. 2003 Analysis of a bifurcation problem in marginally separated laminar wall jets and boundary layers. *Acta Mech.* **161**, 195–211.

Braun, S. & Kluwick, A. 2004 Blow-up and control of marginally separated boundary layer flows. In *New Developments and Applications in Rapid Fluid Flows* (ed. J. S. B. Gajjar & F. T. Smith). *Phil. Trans. R. Soc. Lond.* A (in press).

Braun, S., Kluwick, A. & Trenker, M. 2003 Leading edge separation: a comparison between interaction theory and Navier–Stokes computations. *Proc. Appl. Maths Mech. (PAMM)* **2**, 312–313.

Brown, S. N. & Stewartson, K. 1983 On an integral equation of marginal separation. *SIAM J. Appl. Maths* **43**, 1119–1126.

Duck, P. W. 1990 Unsteady three-dimensional marginal separation, including breakdown. *J. Fluid Mech.* **220**, 85–98.

Elliott, J. W. & Smith, F. T. 1987 Dynamic stall due to unsteady marginal separation. *J. Fluid Mech.* **179**, 489–512.

Fisher, R. A. 1937 The wave of advance of advantageous genes. *Ann. Eugenics* **7**, 355–369.

Galaktionov, V. A. & Vazquez, J. L. 2002 The problem of blow-up in nonlinear parabolic equations. *Discrete Continuous Dyn. Syst.* **8**, 399–433.

Gerhold, T., Galle, M., Friedrich, O. & Evans, J. 1997 Calculation of complex three-dimensional configurations employing the DLR-TAU-code. *AIAA Paper* 1997-0167.

Gittler, Ph. & Kluwick, A. 1987 Triple-deck solutions for supersonic flows past flared cylinders. *J. Fluid Mech.* **179**, 469–487.

Hackmüller, G. & Kluwick, A. 1990 Effects of surface geometry and suction/blowing on marginal separation. *Proc. 3rd Intl Congr. Fluid Mech. Cairo 1990* (ed. A. H. Nayfeh & A. Mobarak), vol. 1, pp. 1–6. Cairo University.

Hackmüller, G. & Kluwick, A. 1991 Effects of 3-D surface-mounted obstacles on marginal separation. In *Separated Flows and Jets* (ed. V. V. Kozlov & A. V. Dovgal), pp. 55–65. Springer.

Hocking, L. M., Stewartson, K., Stuart, J. T. & Brown, S. N. 1972 A nonlinear instability burst in plane parallel flow. *J. Fluid Mech.* **51**, 705–735.

Hsiao, C.-T. & Pauley, L. L. 1994 Comparison of the triple-deck theory, interactive boundary layer method, and Navier–Stokes computation for marginal separation. *Trans. ASME J. Fluids Engng* **116**, 22–28.

Kluwick, A. 1989 Marginale Ablösung laminarer achsensymmetrischer Grenzschichten. *Z. Flugwiss. Weltraumforschung* **13**, 254–259.

Korolev, G. L. 1990 Interaction theory and non-uniqueness of separated flows around solid bodies. In *Separated Flows and Jets* (ed. V. V. Kozlov & A. V. Dovgal), pp. 139–142. Springer.

Lighthill, M. J. 1958 *Introduction to Fourier Analysis and Generalised Functions*. Cambridge University Press.

Mary, I. & Sagaut, P. 2002 Large eddy simulation of flow around an airfoil near stall. *AIAA J.* **40**, 1139–1145.

Moffatt, H. K. 2001 The topology of turbulence. In *New Trends in Turbulence. Turbulence: Nouveaux Aspects*. Lecture notes of the Les Houches Summer School, Session 74, 2000 (ed. M. Lesieur, A. Yaglom & F. David), pp. 329–340. Springer.

Pauley, L. L., Moin, P. & Reynolds, W. C. 1990 The structure of two-dimensional separation. *J. Fluid Mech.* **220**, 397–411.

Ruban, A. I. 1981 Asymptotic theory of short separation regions on the leading edge of a slender airfoil. *Izv. Akad. Nauk SSSR: Mekh. Zhidk. Gaza* **1**, 42–51 (Engl. transl. *Fluid Dyn.* **17**, 33–41).

Ruban, A. I. 1983 Stability of preseparation boundary layer on the leading edge of a thin airfoil. *Izv. Akad. Nauk SSSR: Mekh. Zhidk. Gaza* **6**, 55–63 (Engl. transl. *Fluid Dyn.* **17**, 860–867).

Ryzhov, O. S. & Smith, F. T. 1984 Short-length instabilities, breakdown and initial value problems in dynamic stall. *Mathematika* **31**, 163–177.

Samarskii, A. A., Galaktionov, V. A., Kurdyumov, S. P. & Mikhailov, A. P. 1995 *Blow-up in Quasilinear Parabolic Equations*. Walter de Gruyter Expositions in Mathematics **19**.

Schlichting, H. & Gersten, K. 2000 *Boundary Layer Theory*. Springer.

Sherratt, J. A. 1998 On the transition from initial data to travelling waves in the Fisher-KPP equation. *Dyn. Stab. Syst.* **13**, 167–174.

Smith, F. T. 1982 Concerning dynamic stall. *Aero. Q.* **33**, 331–352.

Smith, F. T. & Daniels, P. G. 1981 Removal of Goldstein's singularity at separation, in flow past obstacles in wall layers. *J. Fluid Mech.* **110**, 1–37.

Smith, F. T. & Elliott, J. W. 1985 On the abrupt turbulent reattachment downstream of leading-edge laminar separation. *Proc. R. Soc. Lond.* A **401**, 1–27.

Stewartson, K. 1970 Is the singularity at separation removable? *J. Fluid Mech.* **44**, 347–364.

Stewartson, K., Smith, F. T. & Kaups, K. 1982 Marginal Separation. *Stud. Appl. Maths* **67**, 45–61.

Taniuti, T. & Wei, C.-C. 1968 Reductive perturbation method in nonlinear wave propagation. *J. Phys. Soc. Japan* **24**, 941–946.

Theofilis, V. 2003 Advances in global linear instability analysis of nonparallel and three-dimensional flows. *Prog. Aerospace Sci.* **39**, 249–315.

Velázquez, J. J. L., Galaktionov, V. A. & Herrero, M. A. 1991 The space structure near a blow-up point for semilinear heat equations: a formal approach. *Zh. Vychisl. Mat. i Mat. Fiz.* **31**, 399–411.

Weideman, J. A. C. 2003 Computing the dynamics of complex singularities of nonlinear PDEs. *SIAM J. Appl. Dyn. Sys.* **2**, 171–186.

Zametaev, V. B. 1986 Existence and nonuniqueness of local separation zones in viscous jets. *Izv. Akad. Nauk SSSR: Mekh. Zhidk. Gaza* **1**, 38–45 (Engl. transl. *Fluid Dyn.* **21**, 31–38).